# 國 立 交 通 大 學

## 資 訊 學 院

## 資 訊 工 程 系

## 博士論文

無線網路下以細胞格為主的定位方法

Cell-based positioning methods for wireless networks

研 究 生：朱鴻棋

指導教授：簡榮宏 博士

中華民國九十五年七月

無線網路下以細胞格為主的定位方法

Cell-based positioning methods for wireless networks

研 究 生: 朱鴻棋　　　　Student: Hung-Chi Chu

指導教授: 簡榮宏 博士　　Advisor: Dr. Rong-Hong Jan

國 立 交 通 大 學 資 訊 學 院

資 訊 工 程 系

博 士 論 文

A Dissertation
Submitted to Department of Computer Science
College of Computer Science
National Chiao Tung University
in partial Fulfillment of the Requirements
for the Degree of
Doctor of Philosophy
in
Computer Science
July 2006
Hsinchu, Taiwan, Republic of China

中 華 民 國 九 十 五 年 七 月

# 無線網路下以細胞格為主的定位方法

研究生: 朱鴻棋　　　　　指導教授: 簡榮宏 博士

## 國立交通大學　資訊工程系

## 摘　要

在無線網路下決定節點的座標位置是一個很有挑戰性的問題。這個問題十分的重要，尤其是對於體積很小的節點，如感測節點。因此，有很多的研究都在探討無線網路下的定位問題。節點定位的問題大致可分成兩大類：集中式及分散式定位方法。集中式定位方法需要有中央控管的伺服器，其功能是負責接收節點所偵測資料及其定位的要求，並根據此資訊執行定位演算法以決定節點位置資訊並回傳給發出詢問的節點。此方法的優點是系統架構簡單且節點負擔較輕。但缺點為伺服器與節點間的通訊成本大，且伺服器的運算負載重。另一方面分散式的定位方法，讓節點可以自行完成定位而不需依靠伺服器的協助。本篇論文針對規則及不規則的網路架構下，提出一個利用訊號涵蓋範圍區域重疊的特性來讓節點自行估計目前的位置。節點只需接收來自參考節點的訊框資訊，並根據收集的資訊來執行簡單的運算即可獲得位置資訊。我們討論所提方法的定位能力及對於不同環境下，評估系統的效能。另外，為了進一步提升定位系統的準確度，我們將具單一訊號強度的參考節點改採用具有多重訊號強度

的參考節點。將此改進方法應用於各種嚴苛的狀況，如參考節點損壞、訊號不穩定、訊框封包遺失等，所提出的方法均能維持良好的運作。對於這樣的結果，我們相信將有助於提供一個簡單、準確且低成本的定位系統。

# Cell-based positioning methods for wireless networks

Student: Hung-Chi Chu        Advisor: Dr. Rong-Hong Jan

Department of Computer Science,
National Chiao Tung University

## Abstract

One challenging issue in wireless networks is to determine where a given node is physical located. This problem is especially crucial for very small nodes such as sensor nodes. Therefore, many researchers have given much attention to positioning problem of wireless networks. This problem can be solved by centralized or distributed positioning methods. The centralized positioning methods need a central server to receive the sensed data, accept positioning queries, perform positioning algorithm and reply the coordinate back to the querying node. The advantages of centralized methods are that their system architecture is simple and the computing load of querying node is light. However, both of the communication overhead between central server and querying node and computational load of central server are very heavy. Therefore, the distributed positioning methods are presented to provide a self-positioning mechanism to reduce these defects. This dissertation develops a distributed positioning method using transmission signal overlapping region that called as cell-based positioning method in regular and irregular network structures. The node receives beacon frames from reference node(s) and performs simple operation to estimate its position. We discuss the characteristics of the proposed method and evaluate the performance in different environment. To improve the positioning accuracy, the radio model with multiple power-levels is applied in the proposed positioning method. In critical situations such as reference node failure, unstable radio transmission range and beacon collision, the proposed method still performs well. We believe that the results are useful for designing a simple, accurate, and low cost positioning system for wireless networks.

# Acknowledgements

Special thanks goes to my advisor Professor Rong-Hong Jan for his guidance in my dissertation work. Thanks also to all members of Computer Network Lab for their assistance and kindly helping both in the research and the daily life during these years. Finally, I will dedicate this dissertation to my families for their love and support.

# Contents

# List of Tables

# List of Figures

ix

# Chapter 1

# Introduction

With the rapid progress of the wireless network technology, it is convenient for people to communicate with one another any time and any place. Mobile devices with wireless capability have gradually integrated into our daily life. A variant of the wireless networks is the wireless sensor networks. It integrates both wireless and sensor technology into a small device, called a sensor node. Each sensor node has the ability to monitor the physical world and return the sensed information to control nodes via wireless communication.

Both wireless networks and wireless sensor networks can be applied to many location-based applications, such as emergency rescue, location tracking, tour guide [1, 2], points of interest, military surveillance, environmental monitoring, health, home, and commerce [3]. Take a forest-fire detection system for example. A large number of sensor nodes are densely deployed in the forest. They are linked together with radio communication. Each sensor node relays its location and the surrounding environmental information, such as temperature, image, air pressure, wind speed, and so on, to the sink node. The sink node, which is a special sensor node, collects the sensed data and replies to the network manager. Abnormal sensed data will trigger the fire warning procedure. The locations of individual

1

sensors are a necessary part of the sensed data since we want to know the location of forest fire when it occurs.

In radio communication, the location of a mobile node can be determined by several methods, such as angle of arrival (AOA) [4], time of arrival (TOA) [4], time difference of arrival (TDOA) [4], and received signal strength indicator (RSSI). These methods are based on telecommunications technology and need additional network equipment in order to determine a mobile node's location. In recent years, several positioning systems were proposed and implemented to real systems [5] such as global positioning system (GPS) [6], Active Badges [7], Active Bats [8], Cricket [9], RADAR [10], SpotOn [11] and so on. GPS is one of the most popular positioning systems for outdoor environment as so far. The average error of GPS is less then 3 meter. However, these positioning methods are not suitable for wireless sensor networks due to size, cost, and power consumption constraints.

This dissertation develops a positioning method using transmission signal overlapping region that called as cell-based positioning method. The transmission signal overlapping region of reference nodes (RNs) was decided in the deployment stage. Because of dense deployment in wireless sensor networks, the whole sensing field can be divided into several independent regions. Note that the independent region is enclosed by signal coverage of different RNs. Take Figure 1.1 for example, the independent region $C_1$ is enclosed by RN 0, 1 and 6. Similarly, the independent region $B_1$ is enclosed by RN 0 and 1. Therefore, the independent region is helpful location information to narrow down the possible location of a SN with geometric analysis.

However, the centralized cell-based positioning method increases the communication overhead for positioning query and the centralized location sever will be

| Regions | RNs Id |
|---------|--------|
| $A_1$ | 0 |
| $B_1$ | 0, 1 |
| $B_2$ | 0, 2 |
| $B_3$ | 0, 3 |
| $B_4$ | 0, 4 |
| $B_5$ | 0, 5 |
| $B_6$ | 0, 6 |
| $C_1$ | 0, 1, 6 |
| $C_2$ | 0, 1, 2 |
| $C_3$ | 0, 2, 3 |
| $C_4$ | 0, 3, 4 |
| $C_5$ | 0, 4, 5 |
| $C_6$ | 0, 5, 6 |
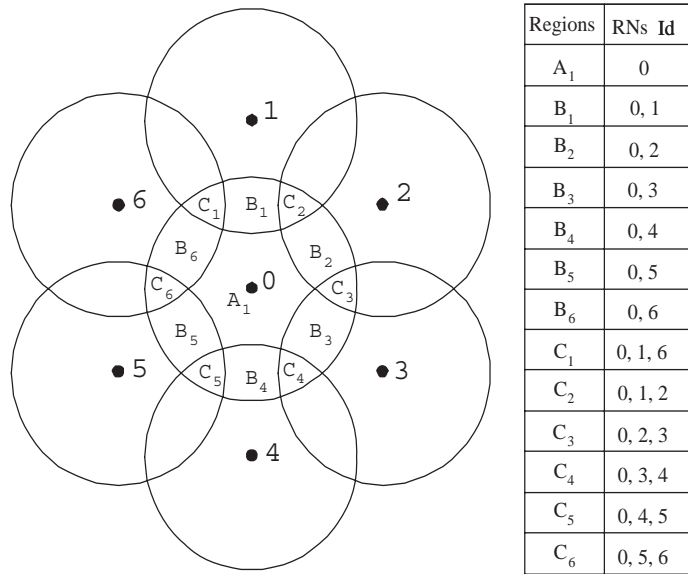
Figure 1.1: The independent regions that enclosed by signal overlapping in cell-based positioning method.

the communication bottleneck under a larger number of positioning queries. A distributed cell-based positioning method is proposed to avoid these defects. Each SN receives the beacon frames transmited by audible RNs. The beacon frame contains the RN's identification (ID) and coordinate. For enough sampling time, SN collects beacon frames to recognize where independent region it is and then estimates its location in the centroid of the independent region. The advantage of this method is that it can solve the defects of centralized cell-based positioning method and the location of sensor node can be estimated by itself with little computation. This kind of positioning system, with its low cost and easy computation, is very suitable for sensor networks.

Finally, to improve the positioning accuracy, an extension of distributed cell-based positioning method using transmission signal overlapping region and multiple transmission power levels is discussed. We know that as the size of independent

region become smaller, the positioning accuracy improves. Based on the power levels of the transmission signal the whole sensing field can be divided into more and smaller independent regions. This improves the positioning accuracy. Our proposed method is suitable for sensor networks that are constrained in energy consumption, computation power, and device cost. This method also provides good location accuracy.

The remainder of this dissertation is organized as follows. The next chapter summarizes previous efforts in positioning research. Chapter 3 presents the cell-based positioning method for regular and irregular network structures. The analysis of positioning accuracy and improving methods are also presented. The multiple power-levels positioning approach and positioning accuracy analysis are presented in Chapters 4. Finally, a conclusion is given in Chapter 5.

# Chapter 2

# Related Works

There are many positioning methods in wireless networks, which can be divided into two categories, centralized positioning systems and distributed positioning systems. The centralized positioning systems utilize a central server to perform localization process. In contract, node performs localization process by itself for the distributed positioning systems. These positioning systems with its advantage and disadvantage are discussed in the following sections.

## 2.1 Centralized positioning systems

A centralized positioning system has a central server. The server collects the sensed data, accepts location queries, performs positioning algorithm and replies coordinate back to the querying node. The coordinate of a sensor node is obtained from the central server. Several mechanisms have been proposed to determine a node's location by the centralized positioning systems. In AOA, TOA, and TDOA [4], additional devices are used in the network to determine the direction and the time (or time delay) of the signal, which are used to calculate a node's location. Such solutions do not require modifications to mobile devices, but produce less accurate position estimates, and incur more network traffic. In an assisted

GPS (AGPS) [12] system, an assistant server with a reference GPS receiver helps a device with a partial GPS receiver to measure the range and estimate its position. The assistant server which is a more powerful computing platform than a GPS receiver has the ability of obtaining information from the wireless channel. The assistant server communicates with a GPS receiver via a wireless channel to help the receiver quickly and efficiently estimate its location. In RADAR [10], multiple base stations (or reference nodes) convert the received signal strength (RSS) to distance information and use a triangulation method to estimate a node's location. A convex positioning [13] system requires a central server to gather the connection information among all sensor nodes. The server uses the connection information to calculate a node's location. A cell-based positioning system [14] utilizes overlapped radio transmission signals of a transmitter to define several independent regions from working area and a central location server to gather the information of independent regions and then to estimate positions. Although these positioning methods produce acceptable position estimates, three major challenges still remain:
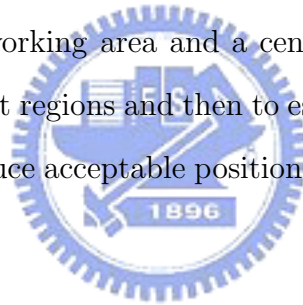
- When the network topology changes, the location of nodes would not be updated immediately. Because of the communication overhead between central server and querying node, it causes long delay for positioning estimation.

- Because the number of usable channels is limited for wireless network, only a few nodes can successfully transmit messages to the central server during a period of time. This situation causes the central server to be the communication bottleneck.

- The positioning of all nodes is estimated by the central server. If the commu-

6

nication link between a node and the central server is broken, the positioning system fails.

## 2.2 Distributed positioning systems

In a distributed positioning system, that is, one without a central server, every sensor node gathers the sensed data and runs a positioning algorithm to estimate its own location. GPS is a typical distributed positioning system [6]. It relies on 24 satellites that orbit around the earth and broadcast precise velocity, latitude, longitude, and altitude information. GPS produces more accurate location estimates but takes longer time to first fix (TTFF) and incur additional cost of setting up a GPS receiver for each sensor node. One mechanism that does not rely on GPS measures the distances among the nodes to build a coordinate system from which relative positions of the nodes can be calculated [15]. The relative positions of nodes were built by the distance of one-hop and two-hop neighbors. Two area-based positioning mechanisms [16, 17] were also proposed by using reference nodes to provide distance information. The reference node is a special-purpose node, which knows its own coordinate and has an unlimited supply of electric power. One mechanism imposes the centroid of selected reference nodes to estimate its own position [16]. The other mechanism narrows down the possible region a node may reside. The region is formed by choosing three reference nodes from all audible reference nodes and tests whether it is inside the triangle formed by these 3 reference nodes. The location of a node will be determined by the center of gravity of the intersection of triangles [17]. In [18], they measure the received signal strength (RSS), communicate with its neighbors, and apply a triangulation method to localize moving sensors and handle dynamically changing sensor

topologies. In [19], a ring-overlapping approach is proposed. Based on received signal strength indicator, the sensor node can find a intersection area where it resides and use the gravity of the intersection area as its position. Niculescu and Nath introduced an ad hoc positioning system using GPS-like triangulation for estimating nodes' locations via distance-vector routing [20] or AOA [21] for range measurement. Based on multidimensional scaling (MDS), Shang et al. used the connectivity information to derive the locations of the nodes [22]. In order to reduce the number of reference nodes, a few mobile reference nodes (those which are equipped with the GPS capability) broadcast their current positions periodically. Other sensor nodes use the information to estimate their own locations [23]. All of the above distributed positioning systems produce acceptable location accuracy and self-positioning ability but there are some defects:

- In GPS systems, not all sensor nodes can afford the GPS capability. Due to the limitations of sensor nodes in size, cost and power consumption, GPS receivers should be used sparingly. In addition, GPS signal will be blocked in indoor environment to lose efficacy for positioning.

- Owing to the limited computational power of sensor nodes, simpler positioning mechanisms is preferred to more complex ones.

# Chapter 3

# Cell-based positioning method with single power-level of RNs

In this chapter, the cell-based positioning method is presented. The circle-shaped area covered by the reference node (RN) is called as a *cell*. That is, one assumes perfectly spherical radio propagation for this idealized model and identical transmission range for all reference nodes[1]. Consider that a set of reference nodes are deployed in the sensor network with overlapping regions of coverage. They are located at known positions in deployment stage.

The sensor node (SN) can receive radio signals containing the RNs' information, if it is within the radio coverage of that RN. Based on the information of RN that SN collect, the positioning of SN can be determined.

In cell-based positioning method, a set of RNs are also deployed in the sensor network with overlapping regions of coverage. They are located at known positions. As shown in Figure 3.1(a), these RNs form a hexagonal structure. A sensor node (SN) in region $C_1$ can listen to signals from RNs $P_0$, $P_1$ and $P_6$; in region $B_1$, from RNs $P_0$ and $P_1$; and in region $A_1$, from RN $P_0$. We define an indepen-

---

[1]This idealized model has been checked by experimental measurements for its validity in [16]. They concluded that the idealized radio model may be considered valid for outdoor unconstrained environments

dent region as one in which every SN in the region receives a unique set of RNs'
signals. The coverage of RN $P_0$ has 13 independent regions, i.e., all the regions
$A_1, B_1, \ldots, B_6, C_1, \ldots, C_5$ and $C_6$. These regions can be classified into three types:

- Type 1 region: The region is covered by only one RN's signal, e.g., region
  $A_1$.

- Type 2 region: The region is covered by two RNs' signal coverage, e.g.,
  regions $B_1$, $B_2$, $B_3$, $B_4$, $B_5$, and $B_6$.

- Type 3 region: The region is covered by three RNs' signal coverage, e.g.,
  regions $C_1$, $C_2$, $C_3$, $C_4$, $C_5$, and $C_6$.
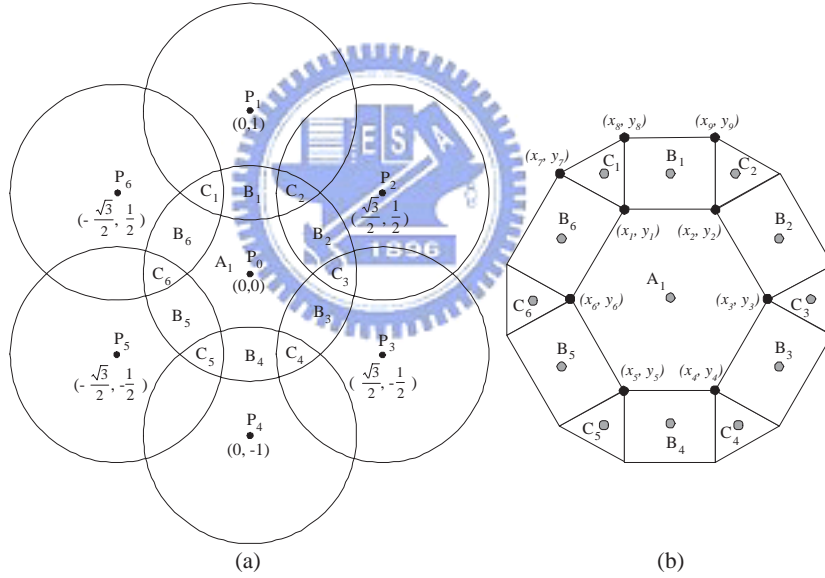


Figure 3.1: The physical layout of RNs with a hexagonal structure for distributed
cell-based positioning method.

Note that the radio coverage of RN is represented as a circle. By using simple
geometry, we can find all the intersections of the circles. For each independent

Table 3.1: The centroids of all regions in the hexagonal network structure.

| Region | Centroid | Region | Centroid |
|--------|----------|--------|----------|
| $A_1$ | $(0, 0)$ | $C_1$ | $(-\frac{\sqrt{3}}{6}, \frac{1}{2})$ |
| $B_1$ | $(0, \frac{1}{2})$ | $C_2$ | $(\frac{\sqrt{3}}{6}, \frac{1}{2})$ |
| $B_2$ | $(\frac{\sqrt{3}}{4}, \frac{1}{4})$ | $C_3$ | $(\frac{\sqrt{3}}{3}, 0)$ |
| $B_3$ | $(\frac{\sqrt{3}}{4}, -\frac{1}{4})$ | $C_4$ | $(\frac{\sqrt{3}}{6}, -\frac{1}{2})$ |
| $B_4$ | $(0, -\frac{1}{2})$ | $C_5$ | $(-\frac{\sqrt{3}}{6}, -\frac{1}{2})$ |
| $B_5$ | $(-\frac{\sqrt{3}}{4}, -\frac{1}{4})$ | $C_6$ | $(-\frac{\sqrt{3}}{3}, 0)$ |
| $B_6$ | $(-\frac{\sqrt{3}}{4}, \frac{1}{4})$ | - | - |

region, we find the centroid $(x_c, y_c)$ of the region by

$$(x_c, y_c) = (\frac{x_1 + x_2 + ... + x_n}{n}, \frac{y_1 + y_2 + ... + y_n}{n})$$

where $(x_1, y_1)$, $(x_2, y_2)$, ..., $(x_n, y_n)$ are the vertices of the region. If a SN can localize itself in the region, we use $(x_c, y_c)$ to estimate the location of the SN. For example, as shown in Figure 3.1(b), if a SN localizes itself in region $B_1$, the estimated location of SN is $(\frac{x_1+x_2+x_8+x_9}{4}, \frac{y_1+y_2+y_8+y_9}{4})$.

Given a set of RNs deployed in a hexagonal structure in which the distance between two neighboring RNs is one unit and the transmission range of RN is $R = 0.78$, we can find the centroids for all localization regions. The results are summarized in Table 3.1.

As stated in the previous description, we can deploy RNs in a hexagonal structure and find the localization regions for each RN. The RN periodically broadcasts the beacon frame to notify all of the SNs staying in its signal coverage area. We assume that each RN knows all centroids of its localization regions. For example, RN $P_0$ knows the centroids of 13 localization regions. The centroids can be computed

in the deployment stage. The beacon format contains the following data:

$$S = \{t_n, (t_{r_a}, \{(x_{c_1}, y_{c_1}), \ldots, (x_{c_a}, y_{c_a})\}), \ldots,$$

$$(t_{r_k}, \{(x_{c_1}, y_{c_1}), \ldots, (x_{c_k}, y_{c_k})\})\}.$$

where $t_n$ represents the type of RN's structure, (e.g., $t_n = 1$ for hexagonal structure and $t_n = 2$ for meshed structure); $t_{r_i}$ represents the type of localization region (e.g., $t_{r_i} \in \{1, 2, 3\}$ for hexagonal structure); and $(x_{c_i}, y_{c_i})$ represents the centroid of the region. Note that the type number of the region is equal to the number of signals that can be received in that region.

For example, as shown in Figure 3.2, the beacon frames of reference node 5 and 6 are

$$S_5 = \{1, (1, \{M\}), (2, \{B, D, F, H, J, L\}),$$

$$(3, \{A, C, E, G, I, K\})\}.$$

$$S_6 = \{1, (1, \{W\}), (2, \{J, N, P, R, T, V\}),$$

$$(3, \{K, I, O, Q, S, U\})\}.$$

where the symbols $A, B, \ldots, W$ represent the centroids of localization regions (e.g., $M = (\frac{\sqrt{3}}{2}, \frac{1}{2}), W = (0, 0)$).

Then, the SN collects the beacon signals from the RNs and determines its location. The operations of SN are given as follows.

1. Collect and store the beacon signal that it receives.

2. Determine the number of RNs, denoted as $m$, that it can listen to. Then extract the centroid set with the type $m$ from the beacon frames , denoted as $S^m$. Note that we can find $m$ different centroid sets. For example, if a SN

12
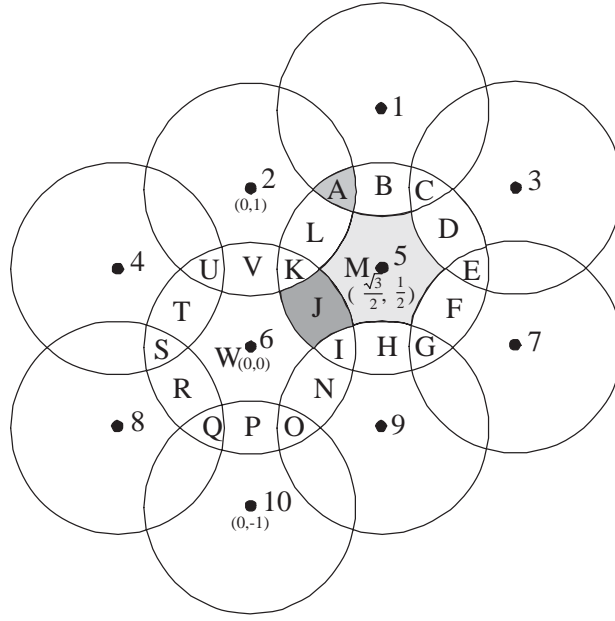
Figure 3.2: An example of localization regions for hexagonal structure.

can receive beacons from RN 5 and 6, it extracts the centroid set with type 2 from the received beacon frames as follows.

$$S_5^2 = \{B, D, F, H, J, L\}.$$
$$S_6^2 = \{J, N, P, R, T, V\}.$$

3. The SN finds a centroid by intersecting the centroid sets as its location, i.e., find $\bigcap_i S_i^m$. For example,

$$
\begin{aligned}
S_5^2 \bigcap S_6^2 &= \{B, D, F, H, J, L\} \bigcap \{J, N, P, R, T, V\} \\
&= \{J\} \\
&= \{(\frac{\sqrt{3}}{4}, \frac{1}{4})\}.
\end{aligned}
$$

In the following, we analyze the positioning accuracy for regular and irregular

13

network structures in chapter 3.1 and chapter 3.2, respectively. After that, an implementation of the proposed method is presented in chapter 3.3.

## 3.1  Positioning accuracy analysis in regular network structure

The evaluation of system performance for positioning method is decided by positioning accuracy. According to analysis the worst-case and average-case positioning accuracy with regular network structure in chapter 3.1.1, it shows the practicality of the proposed method. Furthermore, considering the robustness of the cell-based positioning method, the positioning accuracy for unstable radio propagation model and imperfect reference nodes are discussed in chapter 3.1.2 and 3.1.3, respectively. Finally, the proposed method with backup reference nodes is considered for preventing failure of RNs in chapter 3.1.4.
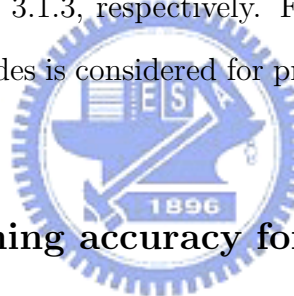
### 3.1.1  Positioning accuracy for perfect reference nodes

Let the coordinate of the actual location of SN be $(X, Y)$ where $X$ and $Y$ are random variables. In the cell-based positioning method, the SN localizes itself to the centroid of the localization region. Thus, the error distance $D$ is

$$D = \sqrt{(X - x_c)^2 + (Y - y_c)^2}$$

where $(x_c, y_c)$ is the centroid of the localization region (i.e., the estimated location of the SN). The *accuracy* can be defined as $D/R_{max}$ and $R_{max}$ is the maximum transmission range of RN. (If $D$ is zero then the accuracy is

assigned as zero.) The *precision* $e(r)$ can be defined as the probability that the SN can localize itself within distance $r$. That is,

$$e(r) = P\{D < r\}$$

Assume that the sensor node falls equally likely to any point in the location region $R$. Then, the probability density function $f(x, y)$ of $(X, Y)$ can be written as follows:

$$f(x, y) = \begin{cases} c & \text{if } (x, y) \in R \\ 0 & \text{otherwise} \end{cases}$$

where

$$\int_R \int f(x, y) dx dy = \int_R \int c \, dx dy = 1.$$

This gives

$$c = \frac{1}{\int_R \int \, dx dy} = \frac{1}{\text{area of R}}$$

Therefore, the precision

$$e(r) = P\{D < r\} = \int_{C_r} \int f(x, y) dx dy = \frac{\text{area } C_r}{\text{area of } R}.$$

where

$$C_r = \{(x, y) | \sqrt{(x - x_c)^2 + (y - y_c)^2} < r\} \cap R.$$

1) *The worst-case accuracy*

Now, let us consider the shape of type 1 as shown in Figure 3.3. The precision $e(r)$ is the area of $C_r$ over the area of localization region $R$, if $r$ is less then $r_1$. If $r$ is greater than $r_1$, the precision $e(r)$ is 1. This means that SN can localize itself within distance $r_1$ with probability 1. In other words, if SN localizes itself in the type 1 region and the tolerance of error distance $d$ is greater than $r_1$, the position of SN can be correctly determined. The radius $r_1$ is called
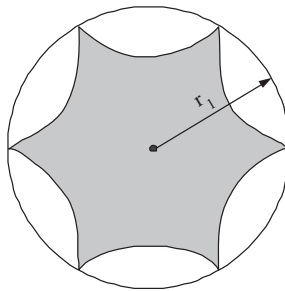
Figure 3.3: The shape of type 1 in hexagonal structure.

the *critical radius*. Furthermore, let $r^* = \max\{r_1^{(1)}, r_1^{(2)}, r_1^{(3)}\}$ where $r_1^{(i)}$ is the critical radius for type $i$ region. Thus, we can say that SN localizes itself correctly within distance $r^*$. Note that $r^*$ is the *worst-case accuracy.*

For example, consider that a set of RNs are deployed in a hexagonal structure in which the distance between two neighboring RNs is one unit and the transmission range of RN is 0.78. We can compute the precision $e_i(r)$ for each type $i$. Figure 3.4 shows the precision $e_i(r)$ for type $i = 1, 2, 3$. Note that $r^* = \max\{r_1^{(1)}, r_1^{(2)}, r_1^{(3)}\} = \max\{0.2685, 0.2993, 0.3088\}=0.3088$. That is, for this hexagonal structure, sensor node localizes itself correctly within distance 0.3088.

Note that critical radius $r_1^{(i)}$ is a function of RN's transmission range $d$. Let $f_i(d)$ be the critical radius for type $i$, $i = 1, 2, 3$. Then, the worst-case accuracy $r^*$ can be rewritten as $r^*(d) = \max\{f_1(d), f_2(d), f_3(d)\}$. If the transmitting power of RN can be adjusted, then the transmission range of RN will vary. We assume that the radius $d$ is bounded within $[\frac{1}{\sqrt{3}}, \frac{\sqrt{3}}{2}]^2$. Let us consider how to arrange the transmission range of RN such that the

---
[2]This is because 1) if $d < \frac{1}{\sqrt{3}}$, then there are some areas not covered by RN's signal; 2) if $d > \frac{\sqrt{3}}{2}$, then the type 2 area will be separated into 2 sub-areas.
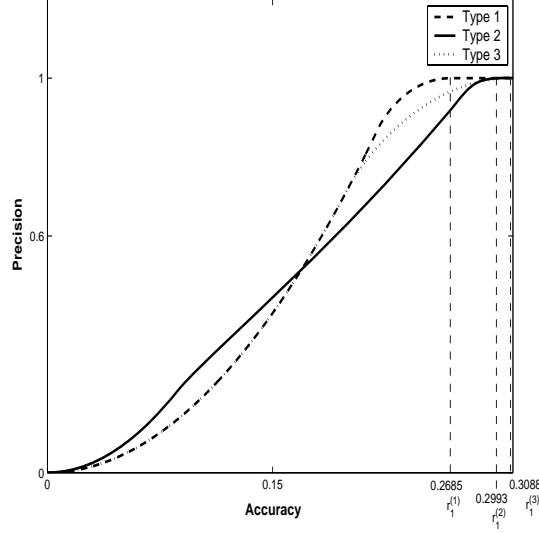
Figure 3.4: The precision $e_i(r)$ of SN in the type 1, 2, and 3 areas.

worst-case accuracy is optimized. This problem is equivalent to finding a radius $d$ such that $r^*(d) = \max\{f_1(d), f_2(d), f_3(d)\}$ is minimized. That is,

$$
\begin{aligned}
z &= \min_{\frac{1}{\sqrt{3}} \leq d \leq \frac{\sqrt{3}}{2}} r^*(d) \\
&= \min_{\frac{1}{\sqrt{3}} \leq d \leq \frac{\sqrt{3}}{2}} \max\{f_1(d), f_2(d), f_3(d)\}
\end{aligned}
\tag{3.1}
$$

Figure 3.5 shows the functions $f_1(d)$, $f_2(d)$, and $f_3(d)$, for $\frac{1}{\sqrt{3}} \leq d \leq \frac{\sqrt{3}}{2}$. The function $f_1(d)$ is a decreasing function and the function $f_3(d)$ is an increasing function where $\frac{1}{\sqrt{3}} \leq d \leq \frac{\sqrt{3}}{2}$. Let $d^*$ be the radius such that $f_1(d^*) = f_3(d^*)$. Thus,

$$
\max\{f_1(d), f_2(d), f_3(d)\} = \begin{cases} f_1(d) & \text{if } \frac{1}{\sqrt{3}} \leq d \leq d^* \\ f_3(d) & \text{if } d^* \leq d \leq \frac{\sqrt{3}}{2} \end{cases}
$$

and the minimum of $\max\{f_1(d), f_2(d), f_3(d)\}$ occurs at $f_1(d) = f_3(d)$. By using the numerical method, we find $d^* = 0.7638$ such that $f_1(d^*) \approx f_3(d^*) = 0.2887$.

17
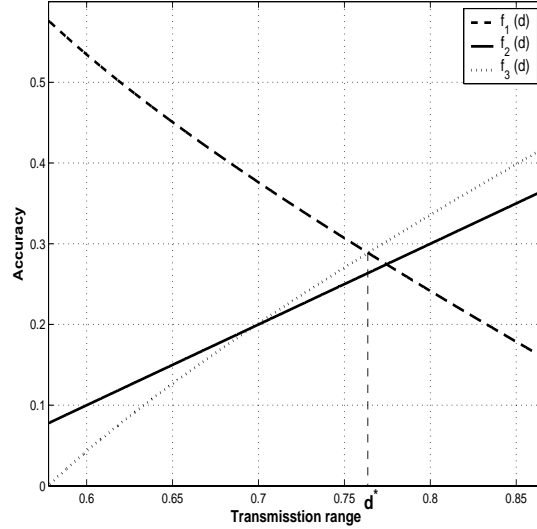
Figure 3.5: The worst-case accuracy for hexagonal structure.

2) *The average-case accuracy*

Given that the location $(x, y)$ of SN falls in the type $i$ area, the expected accuracy $D_i$ is

$$E[D_i] = \int_{(x,y) \in R_i} \sqrt{(x - x_{c_i})^2 + (y - y_{c_i})^2} \; f(x,y) dx dy$$

where $R_i$ is the localization region of type $i$ and $(x_{c_i}, y_{c_i})$ is the centroid of $R_i$. Thus, the expected accuracy of $D$ for the network with hexagonal structure can be found by

$$E[D] = \sum_{i=1}^{3} p_i \; E[D_i]$$

where $p_i$ is the probability that SN falls in the type $i$ area. By this way, we can evaluate the average accuracy of the proposed method.

Note that the average accuracy $E[D]$ is also a function of RN's transmission range $d$. Let $g(d)$ be the average accuracy $E[D]$ for the RNs with hexagonal structure having transmission range $d$. Let us consider how to arrange the

18
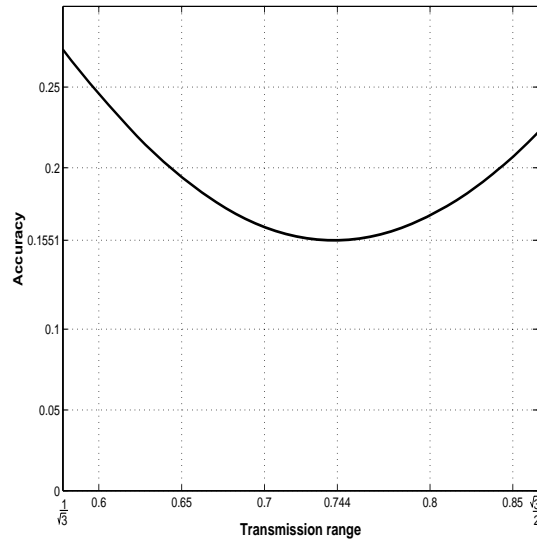
Figure 3.6: The average accuracy for hexagonal structure.

transmission range of RN such that the average accuracy is minimized. The problem is to find a radius $d$ such that $z = \min_{\frac{1}{\sqrt{3}} \leq d \leq \frac{\sqrt{3}}{2}} g(d)$.

We can evaluate the average accuracy $E[D]$ by simulation. In our simulation, 10,000 SNs were generated in the working area of $100 \times 100$ square units. The SNs are placed in the working area with a uniform distribution. We assume that all RNs are deployed in a hexagonal structure with transmission range $\hat{d}$ and their locations are known in advance. By the proposed self-positioning method, each SN can localize itself at position $(x_c, y_c)$. Thus, the positioning error can be found. By this way, we can evaluate the average accuracy $g(\hat{d})$. Furthermore, we find $g(d)$, for $\frac{1}{\sqrt{3}} \leq d \leq \frac{\sqrt{3}}{2}$, as shown in Figure 3.6. Note that function $g(d)$ is a convex function. We find the minimum of $g(d)$ is 0.1551 where $d = 0.744$.

### 3.1.2 Positioning accuracy for unstable radio model

In the previous simulation, we assume the radio is an ideal circle. In reality, the coverage of RN is irregular due to multipath propagation effects. Thus, we construct a simulation using the shadowing model [25] as its radio model. The shadowing model can be represented by

$$[\frac{P_r(d)}{P_r(d_0)}]_{dB} = -10\beta \log(\frac{d}{d_0}) + X_{dB}$$

where $P_r(d)$ $(P_r(d_0))$ is the received signal power at distance $d$ $(d_0)$, $\beta$ is the path loss exponent, and $X_{dB}$ is a Gaussian random variable with $\mu = 0$ and standard deviation $\sigma_{dB}$. Note that the shadowing model extends the ideal circle model to a statistic model. For outdoor environments, we set $\sigma_{dB} = 4$ and $\beta = 2$ (free space) or $\beta = 3$ (shadowed urban area) in our simulation[26]. The SN can receive the beacon frame if the received signal power is greater than the value of $P_r(d)$ where $d$ is 0.744 unit distance. A unit distance is equal to 20 meters in the simulation. The working area was $100 \times 100$ square units and RNs were deployed with hexagonal structure. For randomly generating 100,000 SNs to be located in a working area, Figure 3.7 shows the average accuracy of the proposed method. For outdoor, free space environment (i.e., $(\sigma_{dB}, \beta) = (4, 2)$), the accuracy curve is almost the same as the accuracy curve of perfect model. For outdoor, shadowed urban area (i.e., $(\sigma_{dB}, \beta) = (4, 3)$), the SN can localize itself to within 0.3 unit distance for 89.89% of measurements. Thus, the proposed method still worked well in the outdoor, shadowed urban area.
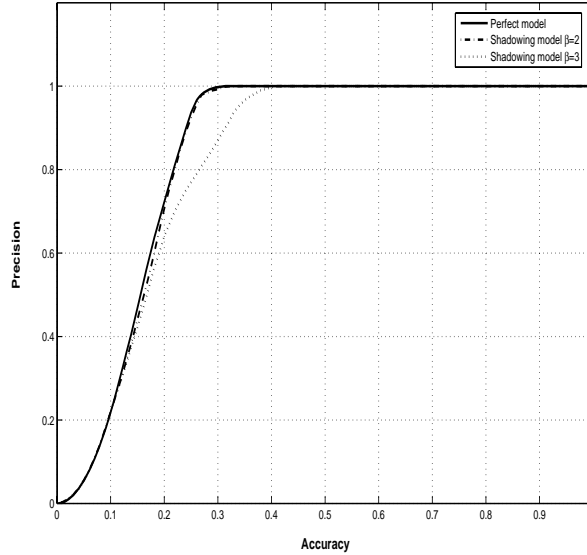
Figure 3.7: The average accuracy for the shadowing propagation model.

### 3.1.3 Positioning accuracy for imperfect reference nodes

In order to show the robustness of the proposed method, we assume that RNs are imperfect. Consider the example given in Section 3. Assume that an SN is in the region $J$ (see Figure 3.2) and RN 6 fails. The SN only receives the beacon frame $S_5 = \{1, (1, \{M\}), (2, \{B, D, F, H, J, L\}), (3, \{A, C, E, G, I, K\})\}$ from RN 5. As a result, the SN localized itself at $M = (\frac{\sqrt{3}}{2}, \frac{1}{2})$. That is, the accuracy error becomes large.

We evaluate the average accuracy for imperfect RN by simulation. In our simulation, 10,000 SNs were generated in the working area of $100 \times 100$ square units. Then, SNs are placed in the working area with a uniform distribution. We assume that all RNs are deployed in a hexagonal structure with transmission range 0.744 and their locations are known in advance. We consider three cases of imperfect RNs. That is, case 1 has a 1% of failure rate of RNs; case 2 has

21
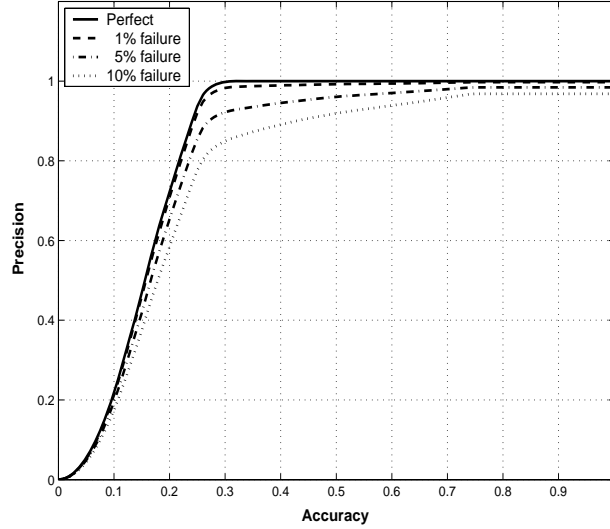
Figure 3.8: The average accuracy for imperfect reference nodes in a hexagonal structure.

5%; and case 3 has 10%. Figure 3.8 shows the average accuracy of the proposed method with imperfect RNs. From Figure 3.8, note that the proposed method with imperfect RNs having 1%, 5%, and 10% failure rates can locate SN to within 0.3088 unit distance for 98.68%, 92.74% and 85.6% of measurements, respectively. Because of the failure of RNs, some SNs in the working area may not localize themselves. When the RNs failure rates are 1%, 5%, and 10%, the probabilities that the SNs can not localize themselves are 0.21%, 1.21%, and 2.36%, respectively. That is, the probability that the SN cannot localize itself is very small and the decease in positioning accuracy is very limited for the network with imperfect RNs having a 10% failure rate.

### 3.1.4 Positioning accuracy for backup reference nodes

For imperfect RNs, it will fail to work in execution stage. When a RN is failed, the entire working area cannot be covered by RNs. In this scenario, the cell-based

22

positioning method is failed to perform positioning in the region that without RNs' signal coverage. Therefore, cell-based positioning method with backup RNs is discussed to avoid unexpectedly failure of RNs. As shown in Figure 3.9, a backup RN $P_{R0}$ is deployed in the centroid of region that can receive thee different RNs' ($P_0$, $P_3$, and $P_4$) signal. The coverage radius of the backup RN is $R_{R0}$ that can cover all type 1 regions of these three RNs (i.e. the shadowed region). In other words, each backup RN is responsible for detecting the status of three RNs so it is deployed in the region that can receive the beacon signal from them. The number of backup RNs is $N/3$ for $N$ RNs.
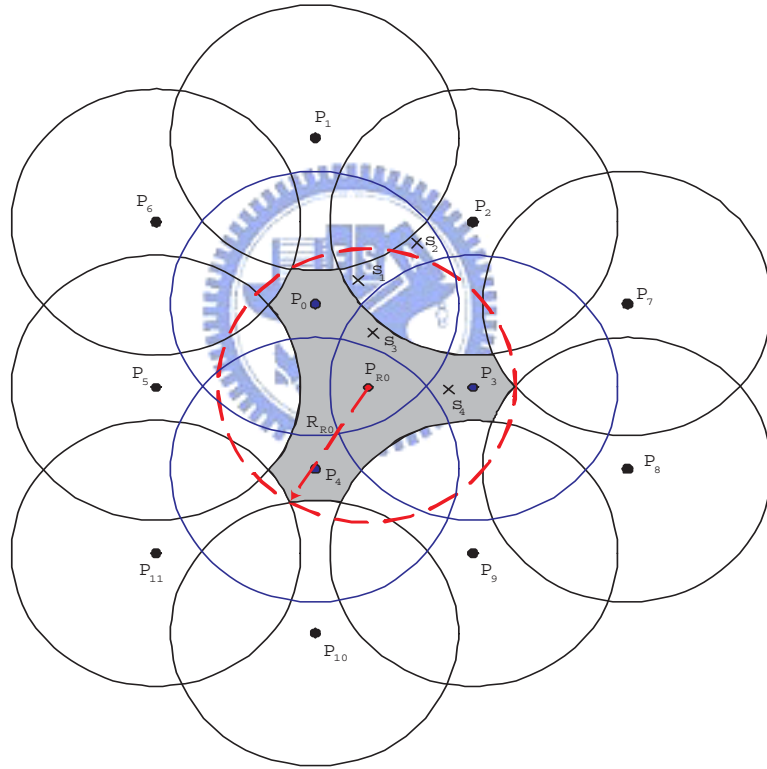


Figure 3.9: The physical layout of cell-based positioning method with backup RNs in hexagonal structure.

A backup RN has two states: *standby* and *active*. In *standby* state, the backup

23

RN receives the heartbeats of RNs to ensure that RNs are perfect. Note that the heartbeat is a periodically message sent from RNs. In the proposed method, the periodical beacon that broadcasts location information of RNs can act as the heartbeat message. In the deployed stage of backup RNs or in the first time receiving RNs' beacon, backup RNs store the content of beacons.

If backup RN cannot receive the heartbeat from any one of these RNs, it changes its state to active. In *active* state, backup RN periodically broadcasts the beacon ($S_f$) that contains the location of failure RN(s). In order to make the beacon format compatible for normal cell-based positioning method that we mentioned in chapter 3.1, the beacon contains the following data:

$$S_f = \{t_n, (x_{fr}, y_{fr}), (f_a, \{(x_a, y_a)\}), \ldots (f_k, \{(x_k, y_k)\})\}$$

where $t_n$ represents the type of RN's structure (e.g. $t_n$=3 for backup structure); $f_i$ represents the status of RN $i$ (e.g. $f_i$=0 for failed RN $i$ and $f_i$=1 for normal RN $i$); $(x_{fr}, y_{fr})$ represents the location of backup RN; and $(x_i, y_i)$ represents the location of RN $i$. Note that the location of failed RN can be obtained from the centroid of type 1 region that contained in the RN's beacon (heartbeat). At the same time, the backup RN sends a notification message that contains the location of failed RN to the manager. After restoring failed RN, the backup RN can receive the heartbeat of RNs. If all heartbeats of RNs in its coverage area can be received by backup RNs, it changes its state to *standby*. The state transition diagram of backup RN is shown in Figure 3.10(a).

According to the state transition of backup RN, SN must transit its current state to corresponding state (see Figure 3.10(b)). If SN receives beacons without backup RN, it performs the cell-based positioning method that we proposed
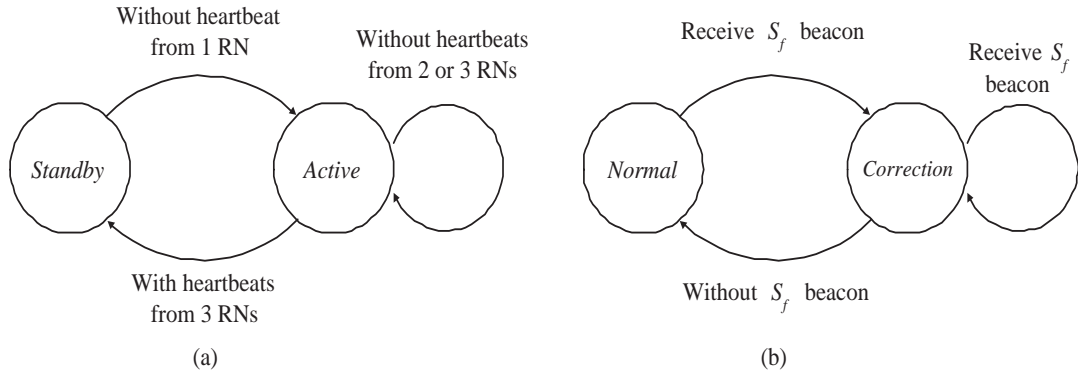
Figure 3.10: The state transition diagram of backup RN and SN. (a)Backup RN has two states: *standby* and *active* (b)SN has two states: *normal* and *correction*

.

in chapter 3. If one or more RNs are failed, SN can receive the beacons form backup RN. SN transits its state from *normal* to *correction* and its position can be evaluated by the following cases:

Case 1: SN received beacons from backup RN but not from other RNs. In this scenario, SN must be located within the shadowed region (See Figure 3.11). Considering the number of failed RNs in the backup RN's coverage area, the location of SN can be discussed by three conditions.

a) *One RN failure*

As shown in Figure 3.11(a), SN is located within the shaded region that is the type 1 region of the failed RN $P_0$. The position of SN is assigned as the location of the failed RN $P_0$.

$$(x, y) = (x_{P_0}, y_{P_0}).$$

b) *Two RNs failure*

SN is located within the shaded region that is shown in Figure 3.11(b). The

25

position of SN can be assigned as the centroid of this region which is the midpoint of the location of these two failed RNs.

$$(x, y) = (\frac{x_{P_0} + x_{P_3}}{2}, \frac{y_{P_0} + y_{P_3}}{2}).$$

c) *Three RNs failure*

SN is located within the shaded region that is shown in Figure 3.11(c). The position of SN can be assigned as the centroid of this region which is the location of the backup RN $P_{R_0}$.

$$(x, y) = (x_{R_0}, y_{R_0}).$$
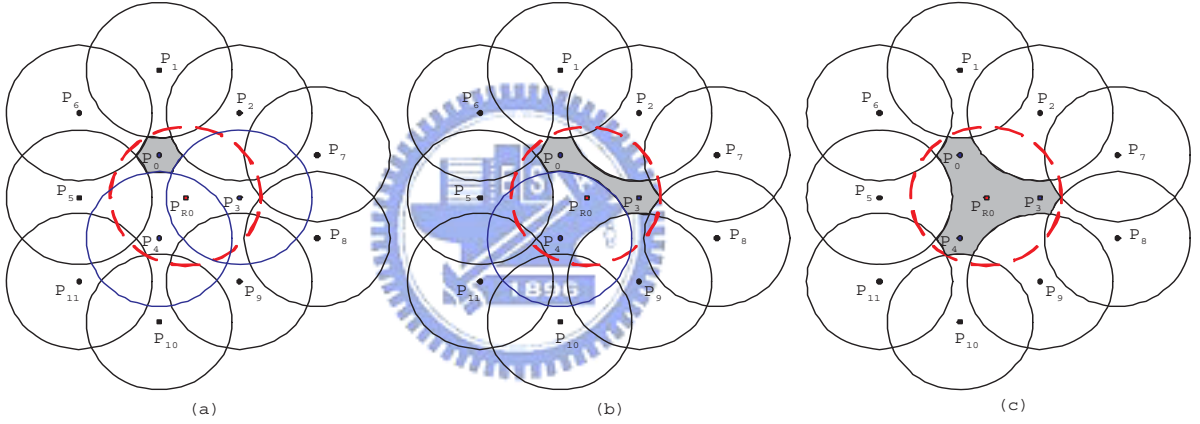


Figure 3.11: The physical layout of 1, 2 and 3 failed RNs with a backup RN $P_{P_0}$. (a)failure of RN $P_0$, (b)failure of RN $P_0$ and $P_3$ (c)failure of RN $P_0$, $P_3$, and $P_4$.

Case 2: SN can receive beacons from backup RN and from one or two RNs. In this scenario, SN is located within the area that includes the coverage area of backup RN $P_{R_0}$ and excludes the region of case 1. The location of SN is decided by the cell-based positioning method without considering the beacons of backup RN for simplicity.

This is because that it is hard to recognize the region where SN is located. For example, RN $P_0$ is failed and four SNs ($s_1, s_2, s_3$, and $s_4$) are located in the sensing area that is shown in Figure 3.9. We know that SN $s_1$ can receive beacons from RN $P_2$ and backup RN $P_{R_0}$ and SN $s_2$ can receive beacons from RN $P_{R_0}$ when RN $P_0$ failed. However, $s_1$ and $s_2$ are located within the same region when $P_0$ is not failed. On the contrary, both SN $s_3$ and $s_4$ can receive beacons from RN $P_3$ and backup RN $P_{R_0}$ when RN $P_0$ failed. However, $s_3$ and $s_4$ are located within different region when RN $P_0$ is not failed. One of the possible solutions is that RN using directional antenna to provide additional information for recognizing these ambiguous regions. This solution has high system complexity and hardware cost. However, considering the simplicity of system, dropping some useful beacons that are broadcasted by backup RN will increase the positioning error. This is a tradeoff between positioning error and system complexity for designing a positioning method. In this dissertation, a simple method with slight positioning error is considered.

We evaluate the average accuracy for backup RNs by simulation. In our simulation, 10,000 SNs were generated in the working area of $100 \times 100$ square units. Then, SNs are placed in the working area with a uniform distribution. We assume that all RNs are deployed in a regular hexagonal structure with transmission range 0.744 and their locations are known in advance. For each three neighboring RNs, one backup RN are placed in the centroid of type 3 region that formed by these three RNs. Three cases of imperfect RNs that proposed in previous section is considered. That is, case 1 has a 1% of failure rate of RNs; case 2 has 5%; and case 3 has 10%. Figure 3.12 shows the average accuracy of the proposed method for imperfect RNs with and without perfect backup RNs. From Figure 3.12, note that

27

the proposed method for imperfect RNs with (without) backup RNs having 1%, 5%, and 10% failure rates can locate SN to within 0.3088 unit distance for 98.89% (98.68%), 93.91% (92.74%) and 87.79% (85.6%) of measurements, respectively. In Figure 3.13, it shows the average accuracy with imperfect RNs (i.e. backup RNs are also imperfect). The number of un-located SNs with and without backup RNs is listed in Table 3.2. The proposed method with backup RNs can reduce the number of un-located SNs from 21, 121 and 236 to 1, 16, and 63 in 1%, 5%, and 10% RNs failure rate, respectively.
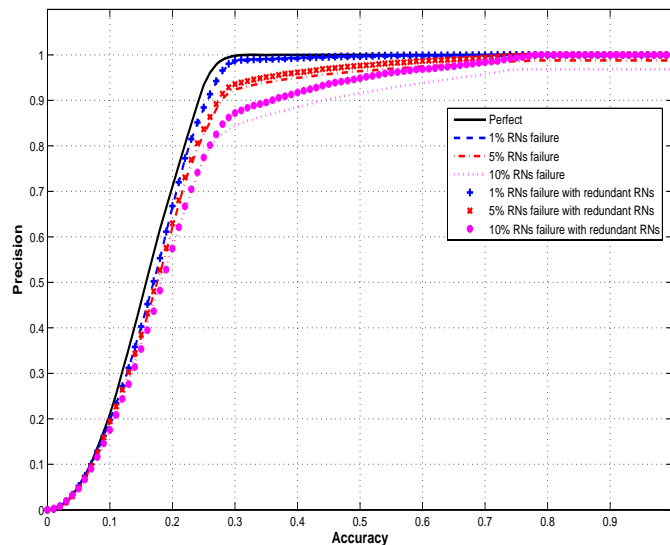


Figure 3.12: The average accuracy for backup RNs in a hexagonal structure (backup RNs are perfect).
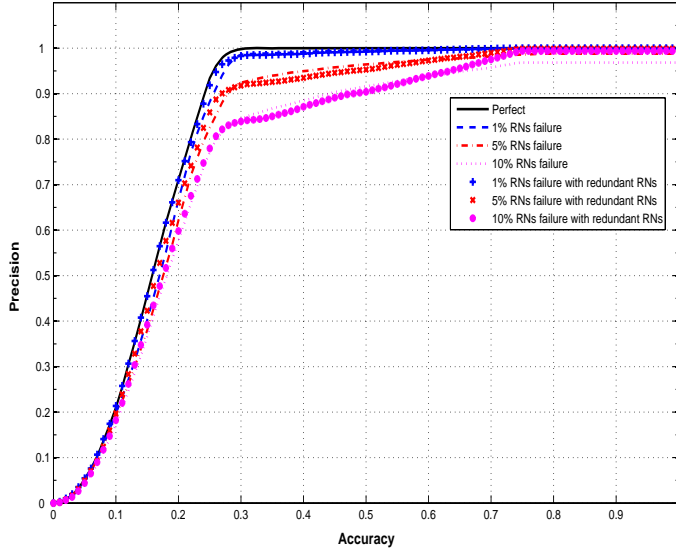
Figure 3.13: The average accuracy for backup RNs in a hexagonal structure (RNs and backup RNs have the same failure rate).

## 3.2 Positioning accuracy analysis in irregular network structure

This section considers a wireless network with $n$ RNs in which the location of $RN_i$, $(x_i, y_i)$ and its transmission range, $r_i$, are given where $i = 1, 2, ..., n$. The radio coverage of $RN_i$ is denoted as circle $C_i$. By using simple geometry, we can find all the intersections of all the circles. Then, we can formulate the positioning

Table 3.2: The number of un-located SNs for the proposed method with and without backup RNs.

| RNs failure | Without backup RNs | With backup RNs |
|---|---|---|
| 1% | 21 | 1 |
| 5% | 121 | 16 |
| 10% | 236 | 63 |

29
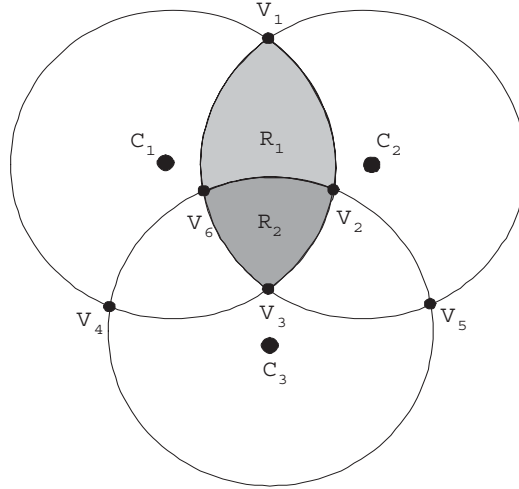
Figure 3.14: A geometry graph $G$.

accuracy problem into a *geometry graph model* $G = (V, E)$. Each vertex in set $V$ stands for intersection points of $C_i$ and $C_j$, and an arc $(u, v)$ is in $E$ if $(u, v)$ is a simple segment of the circle where a simple segment means there is no intersection point between $u$ and $v$. We called a vertex $v$ as a border vertex if $v$ is not inside another circle. An arc $(u, v)$ is called a border arc if both $u$ and $v$ are border vertices. For example, a wireless network as shown in Figure 3.14 can be represented by the graph $G = (V, E)$, where $V = \{v_1, v_2, \ldots, v_6\}$ and $E = \{(v_1, v_2), (v_2, v_3), (v_3, v_4), (v_4, v_1), \ldots, (v_5, v_4), \ldots, (v_2, v_5)\}$. Vertices $v_1, v_4$ and $v_5$ are border vertices and arcs $(v_1, v_4), (v_4, v_5)$ and $(v_5, v_1)$ are border arcs. Note that the localization region $R_1$ is bounded by a set of arcs $(v_1, v_2), (v_2, v_6), (v_6, v_1)$. Thus, the problem of finding the accuracy for the cell-based positioning method is equivalent to finding the maximum size of a localization region in the graph $G = (V, E)$. An algorithm is presented below for finding all localization regions of $G$ and calculating their areas. Therefore, the maximum size of a localization region can be determined.
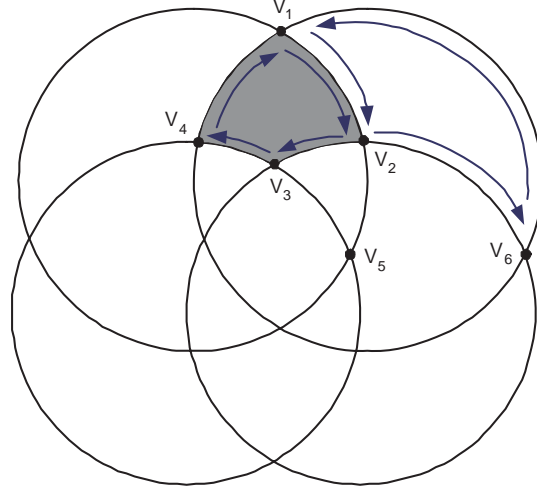
Figure 3.15: A simple cycle search in clockwise direction.

### 3.2.1 Region-finding algorithm

Let $Adj[u]$ denote the adjacency list of $u$. That is, $Adj[u]$ consists of all the vertices adjacent to $u$ in $G$. For two vertices $v_1, v_2 \in Adj[u]$, we define angle $\angle v_1 u v_2$ to be the angle from arc $(v_1, u)$ to arc $(v_2, u)$ in a counter-clockwise direction. A cycle $P_i = (v_{i_1}, v_{i_2}), \ldots, (v_{i_k}, v_{i_1})$ is called a *simple cycle* if it forms a localization region. A simple cycle can be found by the following search procedure. Start to search from any arc $(u, v)$ and set $P_i = (u, v)$. The following arc $(v, v_{j_1^*})$, $v_{j_1^*} \in Adj[v] \backslash \{u\}$, can be chosen into $P_i$ is the arc with minimum angle $\angle uvv_{j_1^*}$. (i.e., $\angle uvv_{j_1^*} = \min_{v_{j_1} \in Adj[v] \backslash \{u\}} \angle uvv_{j_1}$). Now, $P_i = (u, v), (v, v_{j_1^*})$. Next, consider arc $(v, v_{j_1^*})$ and find the following arc $(v_{j_1^*}, v_{j_2^*})$ for $P_i$ such that $\angle vv_{j_1^*}v_{j_2^*} = \min_{v_{j_2} \in Adj[v] \backslash \{u\}} \angle vv_{j_1^*}v_{j_2}$. Repeat the same procedure until the vertex $u$ is reached. Then, a simple cycle $P_i = (u, v), (v, v_{j_1^*}), \ldots, (v_k^*, u)$ is found. For example, as shown in Figure 3.15, start from $(v_1, v_2)$. The next arc selected is $(v_2, v_3)$. This is because $\angle v_1 v_2 v_3 < \angle v_1 v_2 v_5 < \angle v_1 v_2 v_6$. Similarly, choose $(v_3, v_4)$ as the next arc of $(v_2, v_3)$. By this way, a simple cycle $(v_1, v_2), (v_2, v_3), (v_3, v_4), (v_4, v_1)$ is found.

31

Note that such a simple cycle found is in a clockwise direction relative to arc $(u, v)$. Similarly, we can also find another simple cycle for $(u, v)$ in a counter-clockwise direction. This can be done by selecting the next arc $(v, v_{i_1^*})$ of $(u, v)$ such that $\angle uvv_{i_1^*} = \max_{v_{i_1} \in Adj[v] \setminus \{u\}} \angle uvv_{i_1})$. Repeat this procedure until the vertex $u$ is reached. For example, simple cycle $(v_1, v_2), (v_2, v_6), (v_6, v_1)$ was found by a counter-clockwise search.

Suppose that for a given graph $G$, it has $\ell$ simple cycles. Let $P_i = (v_{i_1}, v_{i_2}), \ldots, (v_{i_k}, v_{i_1}), i = 1, ..., \ell$ denote all simple cycles in $G$. Observing these cycles, we found that for any arcs $(v_i, v_j)$ if they are not border arcs, there are two cycles $P_s$ and $P_t$ containing it; otherwise only one cycle $P_u$ contains it. Thus, we can maintain data structures $counter[(u, v)]$ and $region[(u, v)]$ for each arc $(u, v)$. If $(u, v)$ is not a border arc, $counter[(u, v)]$ is set to 2; otherwise, $counter[(u, v)] = 1$. The $region[(u, v)]$ is a set consists of the localization regions separated by $(u, v)$. For example, if $(u, v)$ separates regions $i$ and $j$, then $region[(u, v)] = \{i, j\}$.

The main idea behind the region finding algorithm is that we search each cycle $i$, $P_i = (v_{i_1}, v_{i_2}), \ldots, (v_{i_k}, v_{i_1})$, to see which forms localization region $i$. Then, for each arc $(u, v)$ in $P_i$, set $counter[(u, v)] = counter[(u, v)] - 1$ and $region[(u, v)] = region[(u, v)] \cup \{i\}$. Note that if all counters of the arcs become zero, then all localization regions are found.

A brief pseudocode for the region finding is given as follows.

```
 0   Procedure LRSEARCH(G = (V, E))
 1     RegionNumber = 0
 2     for all (u, v) ∈ E do
 3       region[(u, v)] = ∅
 4       if (u, v) is not a border arc then counter[(u, v)] = 2
 5           else counter[(u, v)] = 1
 6     for all (u, v) ∈ E do
 7       while counter[(u, v)] ≠ 0 do
 8       begin
 9        if counter[(u, v)] = 1 and region[(v, u)] ⊆ region[(u, w)]
10            then find a simple cycle in counterclockwise direction, say P_i
11            else find a simple cycle in clockwise direction, say P_i
12            (comment: w ∈ Adj[u] with ∠uvw = min_{v_j ∈ Adj[v]\{u}} ∠uvv_j)
13        RegionNumber = RegionNumber + 1
14        for all (u_i, v_i) ∈ P_i do
15            counter[(u_i, v_i)] = counter[(u_i, v_i)] − 1
16            region[(u_i, v_i)] = region[(u_i, v_i)] ∪ {RegionNumber}
17       end
18     return(region[(u, v)])
```

An example to illustrate the above procedure is given in Figure 3.16. After applying lines 7 to 17 of Procedure LRSEARCH to arcs, $(v_1, v_2), (v_2, v_3)(v_3, v_4)(v_4, v_5)(v_5, v_6)$ and $(v_6, v_1)$, the 11 localization regions are found as shown in Figure 3.16. (Note that 13 localization regions will be found after all arcs are considered.) Values in the square represent region number and values along the arcs represent $counter[u, v]$ and $region[(u, v)]$.

## 3.2.2   Improving accuracy with power adjustment

If the transmitting power of the RN can be adjusted, then the coverage of the RN varies. Consider this problem: given a set of RN $i$, $i = 1, \ldots, n$, with a fixed location and its transmission range $r_i, a \leq r_i \leq b$, we want to find a set of transmission ranges $(r_1^*, r_2^*, \ldots, r_n^*)$ such that the positioning accuracy is optimized.
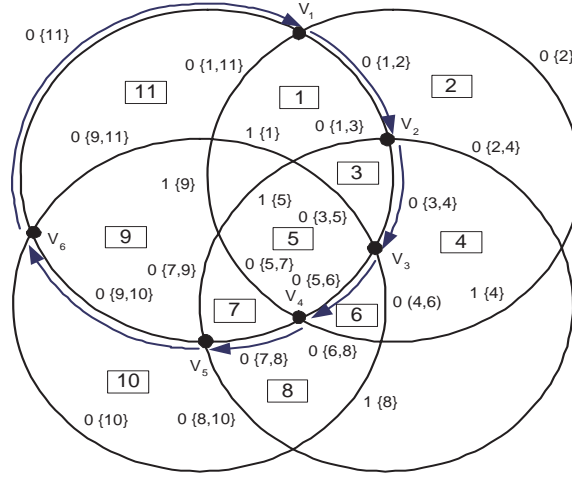
Figure 3.16: An example of region finding.

This problem is equivalent to finding a set of transmission ranges $(r_1^*, r_2^*, \ldots, r_n^*)$ such that $e(r_1, r_2, \ldots, r_n) = \max_{1 \leq i \leq \ell}\{R_i\}$ is minimized. That is,

$$z(r_1^*, r_2^*, \ldots, r_n^*) = \min_{(r_1, r_2, \ldots, r_n)} e(r_1, r_2, \ldots, r_n)$$

where $a \leq r_i \leq b,\ i = 1, 2, \ldots, n.$

In this section, we applied probability analysis to find the optimization solution of power adjustment. However, finding this optimization solution is an NP-hard problem. Therefore, we applied Simulated Annealing (SA) to solve this optimization problem. Finally, we show the improving positioning accuracy with power adjustment by simulation.

*1) Simulated annealing (SA)*

Recently, SA has become more popular for solving large-scale combinatorial optimization problems with approximate optimization solutions. The advantage of SA is that it provides a general purpose solution for a wide variety of combinatorial optimization problems. Thus, SA is used in many fields such as computer-aided de-

34

sign of integrated circuits, image processing, code-designed, neural network theory and so on.

In general, the SA algorithm is similar to metal-cooling. During slow cooling, a metal rearranges the atoms into regular crystalline structures with high density and low energy. The SA algorithm starts with an initial solution $s_0 = (r_1^0, r_2^0, \ldots, r_n^0)$, and finds the value of cost function $e(s_0) = e(r_1^0, r_2^0, \ldots, r_n^0)$, also known as *fitness function*(see equation (1)). Let $s_i$ be the current solution with cost function $e(s_i)$. For each iteration $j$, generate a random neighbor $s_j$ of $s_i$ and evaluate its cost function $e(s_j)$. If $e(s_j) \leq e(s_i)$, then $s_j$ is accepted (i.e., set $s_i = s_j$ and $e(s_i) = e(s_j)$). Otherwise, the $s_j$ will be accepted with the probability $p = \min\{1, \exp((e(s_i) - e(s_j))/T)\}$. The parameter of $T$ means the "temperature" which changed with parameter $\alpha$ for each iteration. This is known as the Metropolis criteria [27] and the pseudocode is shown below:

Step 1: Initialize the temperature $T$. Generate an initial solution $s_0$ and set current solution $s_i = s_0$.

Step 2: Generate a trial solution $s_j$, a random neighbor of $s_i$.

Step 3: Let $\triangle e = e(s_j) - e(s_i)$.

Step 4: If $\triangle e \leq 0$, then the trial solution $s_j$ is accepted. Set current solution $s_i = s_j$ and $e(s_i) = e(s_j)$.

If $\triangle e > 0$, then the trial solution $s_j$ is accepted with the probability $p = \exp(\frac{-\triangle e}{T}) > d$, where $d$ is a random number in $[0, 1]$. Set current solution $s_i = s_j$ and $e(s_i) = e(s_j)$.

Otherwise, go to Step 2.

35
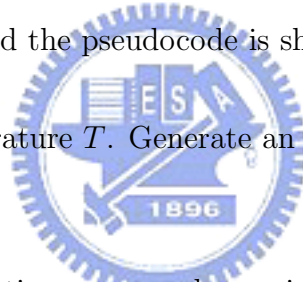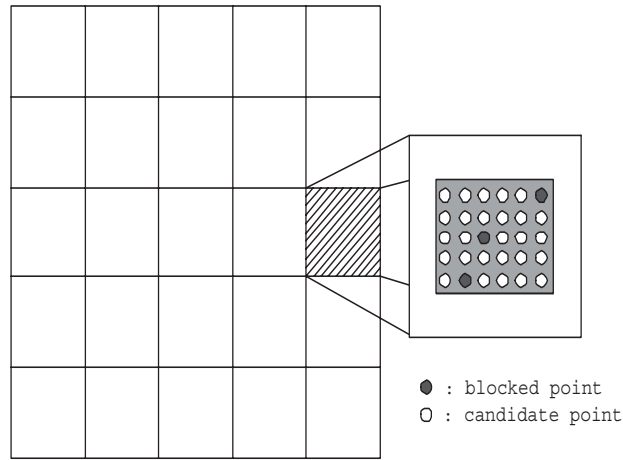
Figure 3.17: Grid-based deployment.

Step 5: Repeat Steps 2-4 for $I_t$ iterations.

Step 6: $T = T \times \alpha$.

Step 7: Repeat Steps 2-6, until $T < T_{stable}$.

In this simulation, we set $I_t = 300, T = 1, T_{stable} = 0.05$ and $\alpha = 0.85$.
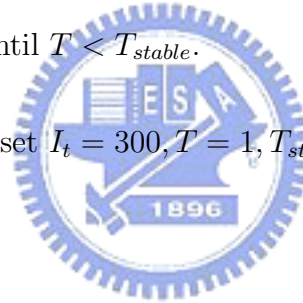
2) *Simulation results*

This simulation ran on networks of $25, 36, 49, \ldots, 225$ RNs in a square working area of 500 units $\times$ 500 units, respectively. We divided the service area into $n$ grids (see Figure 3.17) where $n$ is the number of RNs. As shown in Figure 3.17, white points, called candidate points, represent possible locations to place a RN in the grid. The black points represent block points where one cannot place a RN. Assume that the signal of the RN must cover the entire grid.

Four types of adjustments are considered for improving the accuracy of the cell-based positioning method.

36

Type 1: Assume that the locations of RNs are given and the transmission ranges of the RNs are identical. We evaluate $e(r, r, \ldots, r)$ for $r = a, a + \delta, \ldots, a + k\delta$ where $k = \lfloor \frac{0.6a}{\delta} \rfloor$ and $a$ is the minimal transmission range such that the entire service area is covered. Then find $z(r^*, r^*, \ldots, r^*) = \min\{e(r, r, \ldots, r) | r = a, a + \delta, \ldots, a + \lfloor \frac{0.6a}{\delta} \rfloor \delta\}$. (In our simulation, we set $\delta = 1$.)

Type 2: Assume that the locations of RNs are given and the transmission ranges $r_i, i = 1, 2, \ldots, n$, are in $[a, 1.6a]$. The SA method is applied to the network to find a set of transmission ranges $(r_1^*, r_2^*, \ldots, r_n^*)$ such that $z(r_1^*, r_2^*, \ldots, r_n^*) \approx \min_{(r_1, r_2, \ldots, r_n)} e(r_1, r_2, \ldots, r_n)$.

Type 3: Assume that the transmission ranges $r_i$ $(i = 1, 2, \ldots, n)$ of the RNs are given. SA is applied to the network to allocate the locations $(x_i, y_i)$ of RNs such that $z(r_1, r_2, \ldots, r_n) \approx \min_{(x_1, y_1), \ldots, (x_n, y_n)} e(r_1, r_2, \ldots, r_n)$ where $(x_i, y_i)$ is the coordinate of RN $i$.

Type 4: This is a combination of Types 2 and 3. For a given $(r_1, r_2, \ldots, r_n)$, SA is applied to allocate the locations of RNs. Then, use SA again to adjust the transmission ranges $r_i$ $(i = 1, 2, \ldots, n)$ of the RNs.

Because the optimal value of $z(r_1^*, r_2^*, \ldots, r_n^*)$ is hard to find, we use a lower bound of $z(r_1^*, r_2^*, \ldots, r_n^*)$, denoted as $LB$, for comparison. A lower bound of $z(r_1^*, r_2^*, \ldots, r_n^*)$ is obtained as follows. By simulation, we can estimate the maximum number of localization regions for each network. Then, the whole service area divided by the maximum number of localization regions can be used as a lower bound of $z(r_1^*, r_2^*, \ldots, r_n^*)$. Table 3.3 summarizes the maximum number of localization regions and the lower bound of $z(r_1^*, r_2^*, \ldots, r_n^*)$ for each network.

Table 3.3: The maximum numbers of localization regions and $LB$s of $z(r_1^*, r_2^*, \ldots, r_n^*)$.

| Number of RNs in the network | 25 | 36 | 49 | 64 | 81 | 100 | 121 | 144 | 169 | 196 | 255 |
|---|---|---|---|---|---|---|---|---|---|---|---|
| Maximum number of regions | 168 | 246 | 325 | 416 | 499 | 601 | 673 | 739 | 798 | 865 | 893 |
| $LB$ of $z(r_1^*, r_2^*, \ldots, r_n^*)$ | 1488 | 1016 | 769 | 601 | 501 | 416 | 371 | 338 | 313 | 289 | 280 |

In order to show the performance of the proposed methods, comparisons between the accuracy both before and after the adjustments are made. Let $Z_i$ denote the accuracy $z(r_1^*, r_2^*, \ldots, r_n^*)$ found by Type $i$ and $Z_0$ denote the initial accuracy $e(r_1^0, r_2^0, \ldots, r_n^0)$ where $(r_1^0, r_2^0, \ldots, r_n^0)$ is an initial solution. Figure 3.18 shows the improvement rate $\gamma_i$ of Type $i, i = 1, 2, 4$, where the improvement rate $\gamma_i = \frac{|Z_i - Z_0|}{Z_0} \times 100\%$. Besides, an upper bound of the improvement rate $\bar{\gamma}^* = \frac{|LB - Z_0|}{Z_0} \times 100\%$ is also shown in Figure 3.18. From Figure 3.18, note that the accuracy can be improved up to 30% by the Type 4 method.

Figure 3.19 shows the relationships between the proportion of localization area to the entire service area and the number of RNs in the network. For example, the proportion of the lower bound is $\frac{338}{250000} \times 100\% = 0.14\%$ for the network with 144 RNs. In Figure 3.20, it shows the average accuracy for various numbers of RNs. For Type 1 to 4 with 144 RNs, the average accuracy is within 0.15. In this figure, we learned that increasing the number of RNs from 25 to 144, the accuracy is significantly improved. However, when the number of RNs is more than 144, the improvement of accuracy becomes insignificant.

Finally, the improvement rates of the accuracy of Types 3 and 4 are compared
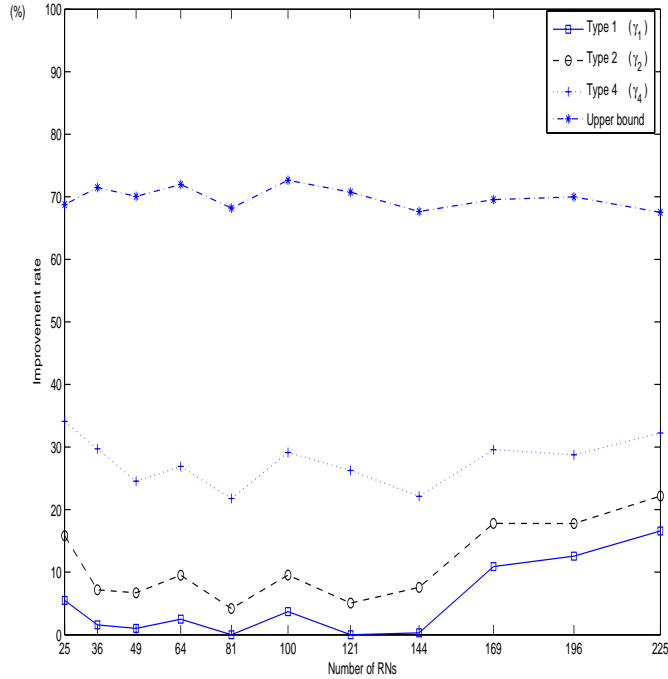
Figure 3.18: The improvement rates of Types 1, 2, and 4, and the upper bound.

in Figure 3.21. The results of the two types are almost the same. This means that for accuracy, the factor of allocating the RNs' locations is more significant than the factor of adjusting transmission ranges. If we can place the RNs in appropriate places, the accuracy of the cell-based positioning method will be better.

## 3.3 Hardware implementation

The proposed self-positioning method was implemented over a collection of MICA2 sensor nodes[28] to verify its feasibility and estimate its accuracy in a real environment. The resource constraints of MICA2 are listed in Table 3.4. We placed MICA2 sensor nodes as RNs on the outdoor skating rink in our campus. The topology is shown in Figure 3.22 in which seven black dots represent seven RNs. The
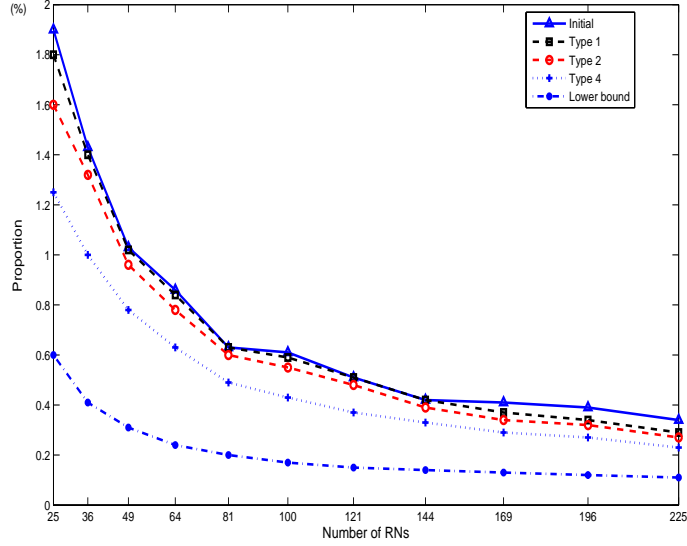
Figure 3.19: The proportion of localization area to the entire service area for various numbers of RNs in the network.

distance between two adjacent RNs is about 10 meters. The transmitting power of each RN was tuned such that its transmission range is about 8 meters. Each RN broadcasts a beacon frame every 200 $ms$. The contents of beacon frames are listed in Table 3.5. The white dot with coordinate $(x, y)$, where $x$ and $y$ are integers, in Figure 3.22 represents a test point. Each time we placed a MICA2 sensor node on a test point (white dot) and then the sensor node collected beacon frames for 9600 $ms$. Let $N_a$ be the total number of beacon frames collected at test point $a$ and $N_a(i)$ be the number of beacon frames collected at test point $a$ that were issued from RN $i$. The sensor node at test point $a$ truncated the beacon frames from RN $i$ if $\frac{N_a(i)}{N_a}$ is less than 0.1. Based on the beacon frames it collected, the sensor node localized itself by the proposed positioning method. In our experiment, we measured 276 test points as shown in Figure 3.22.

Figure 3.23 shows the average accuracy for experiment and simulation results.

40

Table 3.4: The parameters and hardware information about Mote.

| Component | Description |
|---|---|
| Processor | Atmel ATMega 128L |
| Program flash memory | 128K bytes |
| Configuration EEPROM (Data) | 4K bytes |
| Frequency | 868 - 870MHz |
| Radio Transceiver | Chipcon CC1000 |
| Battery | 2 AA batteries |

Table 3.5: The beacon content of RNs.

| RN | Beacon content |
|---|---|
| RN 0 | {1, (1, {(15,15)}), (2, {(15,20),(19,18),(19,13),(15,10),(11,13),(11,18)}), (3,{(12,20),(18,20),(21,15),(18,10),(12,10),(9,15)})} |
| RN 1 | {1, (1, {(15,25)}), (2, {(15,30),(19,28),(19,23),(15,20),(11,23),(11,28)}), (3,{(12,30),(18,30),(21,25),(18,20),(12,20),(9,25)})} |
| RN 2 | {1, (1, {(24,20)}), (2, {(24,25),(28,23),(28,18),(24,15),(19,18),(19,23)}), (3,{(21,25),(27,25),(30,20),(27,15),(21,15),(18,20)})} |
| RN 3 | {1, (1, {(24,10)}), (2, {(24,15),(28,13),(28,8),(24,5),(19,8),(19,13)}), (3,{ (21,15),(27,15),(30,10),(27,5),(21,5),(18,10)})} |
| RN 4 | {1, (1, {(15,5)}), (2, {(15,10),(19,8),(19,3),(15.0),(11,3),(11,8)}), (3,{ (12,10),(18,10),(21,5),(18,0),(12,0),(9,5)})} |
| RN 5 | {1, (1, {(6,10)}), (2, {(6,15),(11,13),(11,8),(6,5),(2,8),(2,13)}), (3,{ (3,15),(9,15),(12,10),(9,5),(3,5),(0,10)})} |
| RN 6 | {1, (1, {(6,20)}), (2, {(6,25),(11,23),(11,18),(6,15),(2,18),(2,23)}), (3,{ (3,25),(9,25),(12,20),(9,15),(3,15),(0,20)})} |
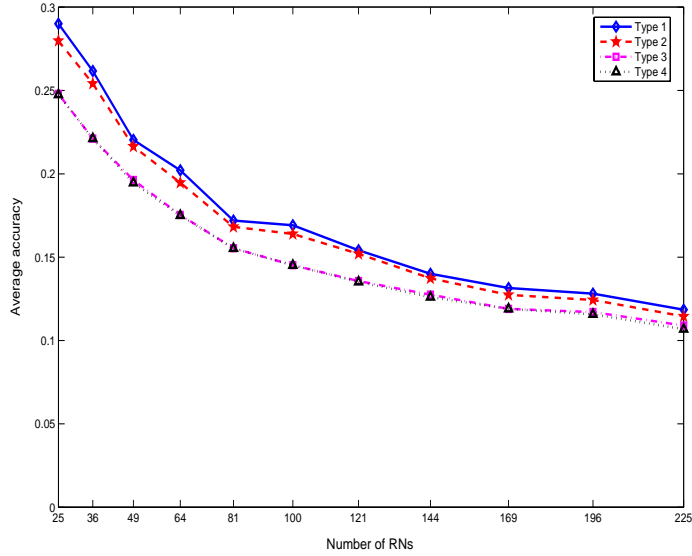
Figure 3.20: The average accuracy for various numbers of RNs.

We defined 10 meters as a unit distance in our experiment. From Figure 3.23 we note that the SN can localize itself to within 0.3 unit distance (i.e. 3 meters) for 91.67% of measurements in our outdoor experiments. The experimental results also agree with simulation results using shadowing model ($\beta = 3$). In Figure 3.24, the positioning error obtained from experiment is plotted as a function of the test point. The positioning error is lowest for the test point at the centroid of the region and increases towards the edges of the region. The average positioning error was 1.79 $m$ and the standard deviation was 0.86 $m$. The minimum error was 0 $m$ and the maximum error was 4.12 $m$ across 276 test points.
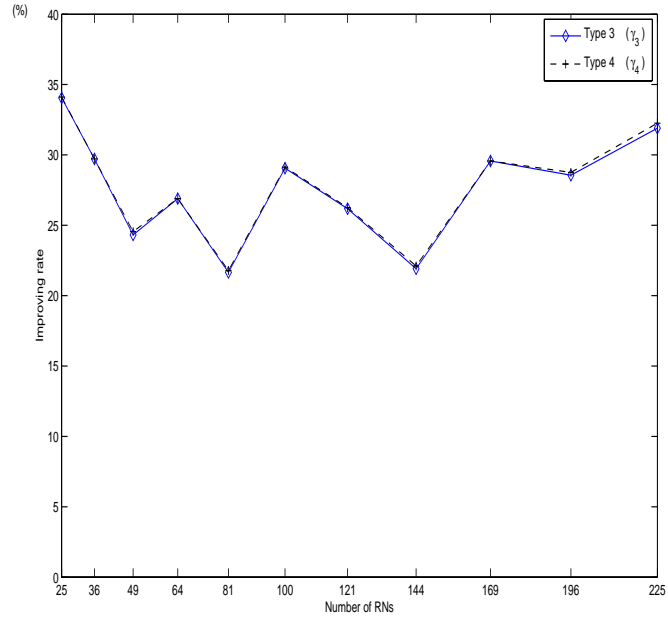
Figure 3.21: The improvement rates of Types 3 and 4.



(a)

(b)
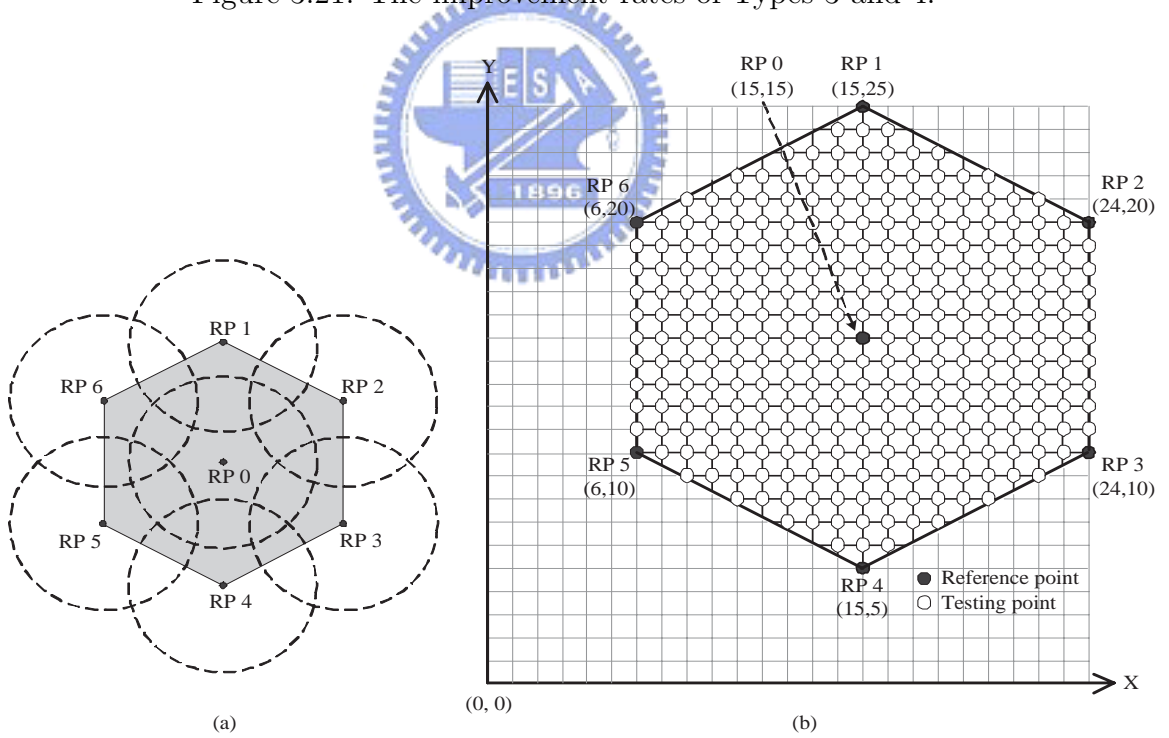
Figure 3.22: The experimental structure.

43
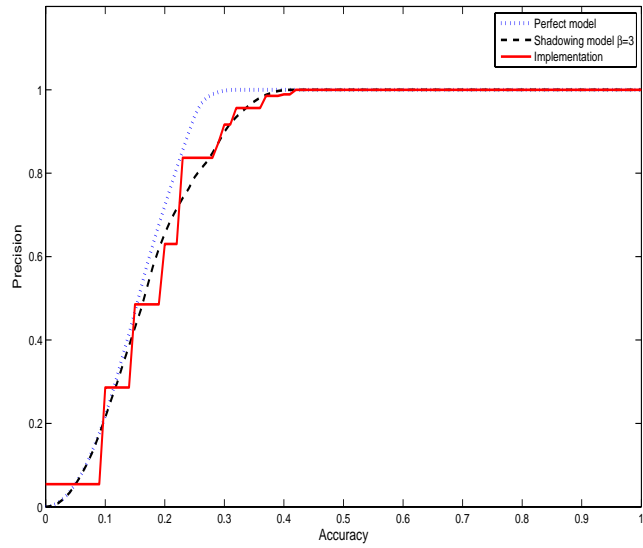
Figure 3.23: The average accuracy for hexagonal structure in the experiment.
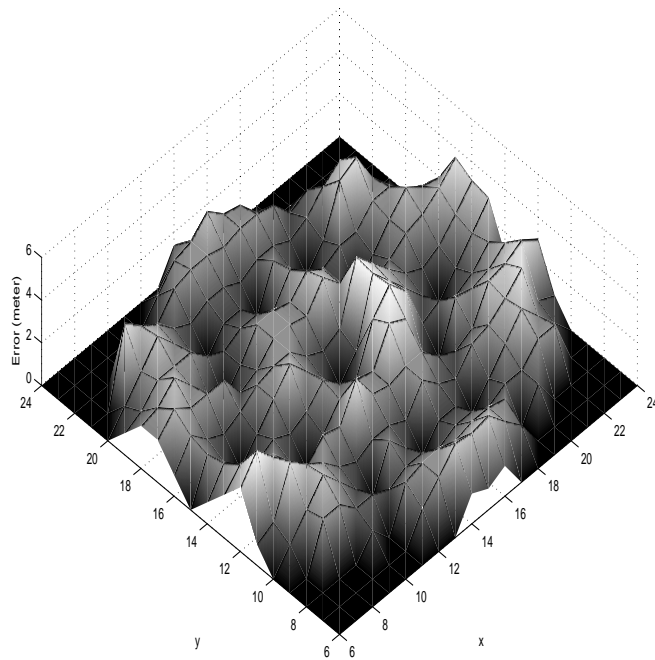


Figure 3.24: The positioning error for all test points.

44

# Chapter 4

# Cell-based positioning method with multiple power-levels of RNs

The signal overlapping technique was used to perform nodes' localization [14]. An extension of the signal overlapping technique with multiple power-levels is used in this method. The basic idea of our multiple power-levels positioning method is that each reference node (RN) periodically broadcasts beacon frames that contain its coordinates, power-levels and current power-level. A RN is a special-purpose sensor node, which knows its own coordinate and has an unlimited supply of electric power. Sensor nodes (SNs) receive the beacon frames to perform localization by themselves.

The proposed localization algorithm can be broken down into four major steps: 1) initial set up, 2) broadcasting beacon frames, 3) processing beacon frames, and 4) computing a node's location. The first two steps are performed at RNs and the last two steps are performed at SNs. The four steps are presented follow:

Step 1: *Initial setup.* Reference nodes are randomly deployed in the sensing area and their positions can be obtained in advance. We assume entire sensing area is jointly covered by all RNs' signals. In Figure 4.1, the coordinates of RNs

1 through 4 are (0, 100), (100, 100), (0, 0), and (100, 0), respectively. Each RN has four power-levels (20, 40, 60, 80).

Step 2: *Broadcasting beacon frames.* Reference nodes periodically broadcast beacon frames that contains the coordinates of RN, RN's multiple power-levels and the current power-level. The beacon frame from RN $i$ contains the following data:

$$S = \{(x_i, y_i), P_i, p_i^c\}$$

where $(x_i, y_i)$ is the coordinate of RN $i$, $P_i$ is the set $\{p_i^1, p_i^2, \dots, p_i^j\}$ of power-levels of RN $i$, and $p_i^c$ represents the power-level of the current frame. Note that $P_i = \{p_i^1, p_i^2, \dots, p_i^j\}$ where $j$ is the maximum number of power-levels and $p_i^c$ is an element of $P_i$. For example, as shown in Figure 4.1, RN 1 has four power-levels (i.e. $j = 4$) and periodically broadcasts different beacon frames for each power-level. The contents of the beacon frames for four power-levels are:

In power-level 1: {(0, 100),(20, 40, 60, 80), 20}.

In power-level 2: {(0, 100),(20, 40, 60, 80), 40}.

In power-level 3: {(0, 100),(20, 40, 60, 80), 60}.

In power-level 4: {(0, 100),(20, 40, 60, 80), 80}.

According to the signal propagation model, the values of power-level can be translated into the signal transmission distances with a formula in[25]. Experimental results of signal propagation for a specific environment can derive the relationship between the signal power-level and the signal transmission distance in real-world applications. In this dissertation, the values of power-levels in beacon frames will denote the signal transmission distances.

In chapter 4.1, we will show how to determine a suitable value for each power-level.

Step 3: *Processing beacon frames.* After each SN receives enough beacon frames for a short period, it estimates its distance from the RN based on the minima of the power-levels of the received beacon frame. For example, assume the beacon frames received by a RN are as follows:

In power-level 2: $\{(0, 100),(20, 40, 60, 80), 40\}$

In power-level 3: $\{(0, 100),(20, 40, 60, 80), 60\}$

In power-level 4: $\{(0, 100),(20, 40, 60, 80), 80\}$.

The SN $A$ can obtain the appropriate power-level by minimizing the current power-level, i.e. $Min\{40, 60, 80\} = 40$. According to the set of power-levels and the appropriate power-level, the estimated distance between RN 1 to SN $A$ is between 20 and 40 units.

Step 4: *Computing a node's location.* Sensor node can gather appropriate power-level from at least one RN. Based on one or more appropriate power-levels, a signal overlapping region can be determined. The positioning of SN can be decided by the approximate centroid of signal overlapping region. The details of node localization process will be discussed in chapter 4.2.

## 4.1   Setting up the optimal power levels

An SN's location is determined from the power levels of the beacon frames. Intuitively, more and finer-grained power levels would result in better estimations at the cost of more delicate electronics in the sensors and more complicated calculation. According to our experiments, there is little marginal advantage when the

47
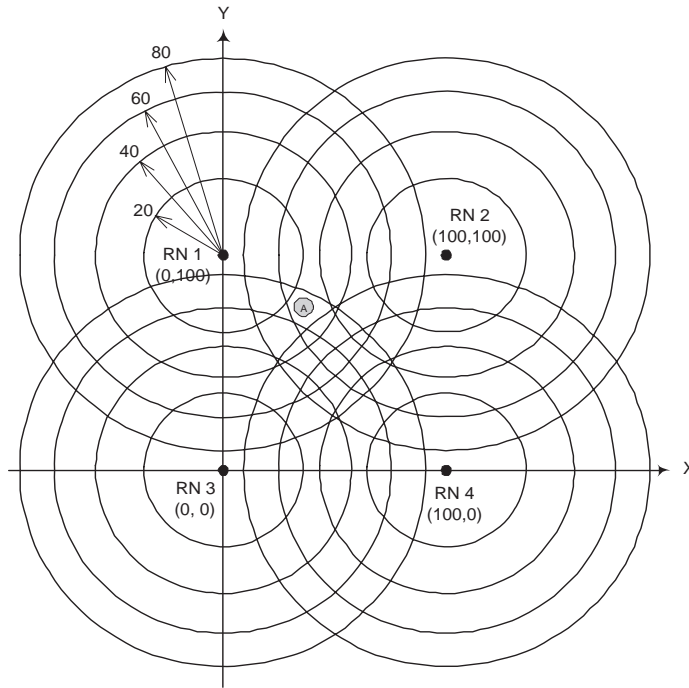
Figure 4.1: An example of localization regions for multiple power-levels structure.

number of power levels exceeds 4.

In Figure 4.1, the differences between adjacent power levels are always a constant (20). However, this is not necessarily the case. In our experiments, we tried several alternatives.

In our testbed, the working area is a $100 \times 100$ square. There is an RN on each of the four corners. 10,000 sensor nodes are deployed in the square area for each unit distance. These SNs are placed at coordinates $(0,0), (0,1), \ldots, (0,99), (1,0), (1,1), \ldots, (1,99), \ldots, (99,0), (99,1), \ldots, (99,99)$. Positions of Sensor nodes are estimated with the proposed localization algorithm and are compared to the actual positions. The average accuracy is a good indication of the overall performance of our localization algorithm. We assume the area covered by a signal is a circle.

In our simulation, the number of power levels ranges from 1 to 7. The power

48

levels range from 1 to 99 ($R_{max} = 99$). The simulation result is shown in Table 4.1. As we mentioned in chapter 3.1.1, the average error is the average error distance $D$ and the average accuracy is defined as $D/R_{max}$, where $R_{max}$ is the maximum transmission range. We can see that, as the number of power levels increase, the average accuracy decreases. When the number of power levels exceeds 4, the reduction in the average accuracy is only marginal.

Table 4.1: Optimal power levels for various numbers of power levels

| Number of power levels | Optimal power levels | Avg. error | Avg. accuracy |
| --- | --- | --- | --- |
| 1 | (81) | 20.0966 | 0.203 |
| 2 | (62,98) | 10.2869 | 0.1039 |
| 3 | (54,79,99) | 7.3186 | 0.0739 |
| 4 | (47,69,85,99) | 5.8686 | 0.0593 |
| 5 | (37,57,76,89,99) | 4.9995 | 0.0505 |
| 6 | (37,54,69,81,91,99) | 4.2993 | 0.0434 |
| 7 | (33,48,63,74,83,91,99) | 3.714 | 0.0375 |

We also used two strategies for testing various power levels: (1) the difference of the powers between adjacent levels is a constant and (2) the ratio of the powers between levels $m + 1$ and $m$ is $\sqrt{m + 1}$. In the latter strategy, it is easy to verify that the rings between adjacent levels cover the same area, as shown in Figure 4.2. The simulation results of the two strategies are shown in Tables 4.2 and 4.3, respectively. The average accuracy of Tables 4.1, 4.2, and 4.3 are plotted in Figure 4.3 for comparison. It is obvious that the second strategy (equal-area rings) approaches the optimal power levels when the number of power levels is 4 and larger. In terms of average accuracy, the second strategy is always better than

49
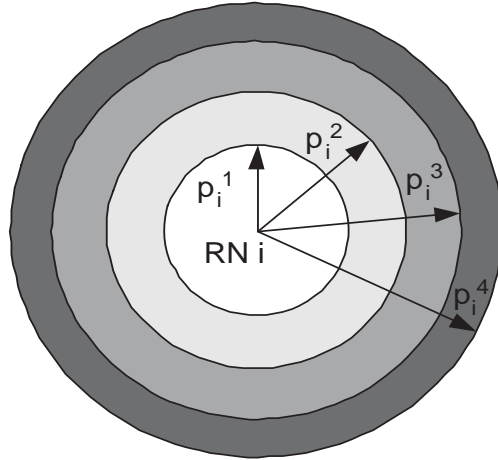
the first.



Figure 4.2: The equal area of ring.

Table 4.2: Power levels for the first strategy

| Number of power levels | Power levels | Avg. error | Avg. accuracy |
|:---:|:---|:---|:---|
| 1 | (99) | 31.2008 | 0.3152 |
| 2 | (50,99) | 15.2251 | 0.1538 |
| 3 | (33,66,99) | 10.5579 | 0.1066 |
| 4 | (25,50,75,99) | 8.6427 | 0.0873 |
| 5 | (20,40,60,80,99) | 7.1742 | 0.0725 |
| 6 | (17,33,50,66,83,99) | 6.0276 | 0.0609 |
| 7 | (14,28,42,57,71,85,99) | 5.6187 | 0.0568 |

## 4.2 Node Localization

An SN determines the ring it is located from the power levels of the beacon frames that it can receive from an RN. When there are multiple RNs, the SN is located

Table 4.3: Power levels for the second strategy

| Number of power levels | Power levels | Avg. error | Avg. accuracy |
|:---:|:---|:---|:---|
| 1 | (99) | 31.2008 | 0.3152 |
| 2 | (70,99) | 12.9954 | 0.1313 |
| 3 | (57,81,99) | 7.8615 | 0.0794 |
| 4 | (49,70,86,99) | 6.0703 | 0.0613 |
| 5 | (44,63,77,89,99) | 5.2614 | 0.0531 |
| 6 | (40,57,70,81,90,99) | 4.4241 | 0.0447 |
| 7 | (37,53,65,75,84,92,99) | 3.9646 | 0.04 |

in the overlapping area of the rings. We will assume the SN is at the centroid of the of the overlapping area. There are four cases to consider:

Type 1: The sensor node receives beacon frames from only one reference node. In this case, the SN is assumed to be at exactly where the RN is since the centroid of a ring is the center of the two circles enclosing the ring. (Note that the RN is located at the center of the circles.)

Take Figure 4.4 for example. SN $A$ is located in the ring whose thickness is proportional to $p_i^m$ and $p_i^{m+1}$, where $p_i^m$ and $p_i^{m+1}$ are the lowest power and the second lowest power of the signals that $A$ can receive from RN $i$, respectively. However, according to this centroid method, the estimated location of $A$ is the centroid of the ring, which is exactly where RN $i$ is. The error of this estimation is proportional to $p_i^m$, rather than the difference $p_i^m - p_i^{m+1}$. When $p_i^m$ is large, the estimation error could be significant. A possible improvement is to use directional antennae for RNs. However, this
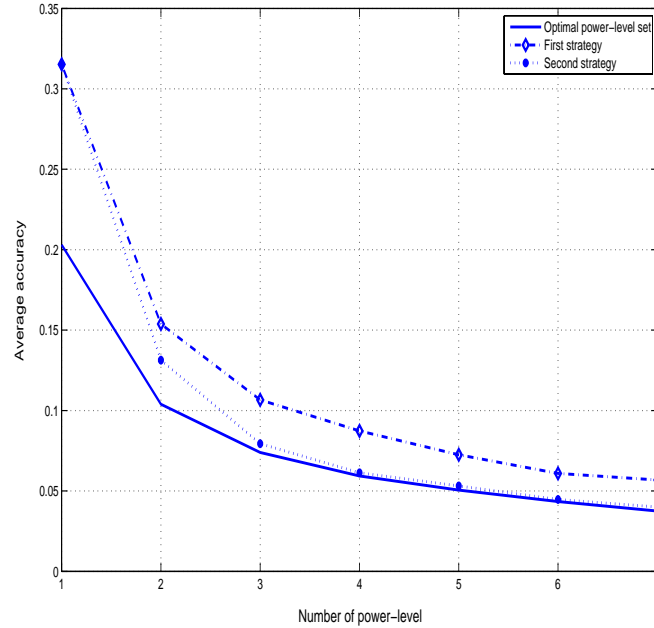
Figure 4.3: The average accuracy of optimal power-level set, first strategy and second strategy.

solution will incur higher cost, more power consumption and more complex systems. In this paper, we only considered omni-directional antennae for simplicity.

Type 2: The sensor node can receive beacon frames from exactly two reference nodes. Let RNs $i$ and $j$ be the two reference nodes. In this case, the estimated position of SN should the centroid of the overlapped region of the two rings determined from the strengths of the signals received from RNs $i$ and $j$. However, computing the exact coordinate of the centroid is too complex a task for a sensor node. We use an approximation.

Consider Figure 4.5. Let $p_i^m$ be the least power level of the beacon frames received from RN $i$. We draw a circle whose center is RN $i$ and whose radius is
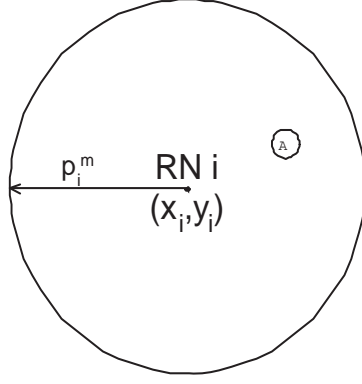
Figure 4.4: Type 1 signal overlapping region.

$p_i^m$. We may draw a similar around RN $j$. The intersection of the overlapped region of the two circles and the line linking RNs $i$ and $j$ is a line segment, denoted $L$ in Figure 4.5. The estimated location of the sensor is taken to be the midpoint of the line segment $L$.

Let the coordinates of RNs $i$ and $j$ be $(x_i, y_i)$ and $(x_j, y_j)$, respectively. Let $(x_e, y_e)$ be the coordinate of the midpoint $M$ of $L$. Thus, we can have the following equation:

$$\begin{cases} x_e = x_i + (x_i - x_j)t \\ y_e = y_i + (y_i - y_j)t, \end{cases} \tag{4.1}$$

The length of the line segment from RN $i$ to midpoint $M$ is $p_i^m - \frac{L}{2}$. Therefore, we have the equation:

$$\sqrt{(x_i - x_e)^2 + (y_i - y_e)^2} = p_i^m - \frac{L}{2} \tag{4.2}$$

Solving Eq. 4.1 and 4.2, we obtain

$$\sqrt{(x_i + (x_i - x_j)t - x_i)^2 + (y_i + (y_i - y_j)t - y_j)^2} = p_i^m - \frac{L}{2}$$

$$\Rightarrow \sqrt{((x_i - x_j)t)^2 + ((y_i - y_j)t)^2} = p_i^m - \frac{L}{2}$$

53

$$\Rightarrow t\sqrt{(x_i - x_j)^2 + (y_i - y_j)^2} = p_i^m - \frac{L}{2}$$

$$\Rightarrow t = \frac{2p_i^m - L}{2\sqrt{(x_i - x_j)^2 + (y_i - y_j)^2}}.$$

Let $\overline{ij}$ be $\sqrt{(x_i - x_j)^2 + (y_i - y_j)^2}$. The coordinate of SN, $(x_e, y_e)$, is

$$x_e = x_i + \frac{(x_i - x_j)(p_i^m - p_j^n + \overline{ij})}{2 \times \overline{ij}}$$

$$y_e = y_i + \frac{(y_i - y_j)(p_i^m - p_j^n + \overline{ij})}{2 \times \overline{ij}}.$$



Figure 4.5: Type 2 signal overlapping region.

Type 3: The sensor node can receive beacon frames from exactly three reference nodes. As shown in Figure 4.6, the position of SN is taken to be the intersection of $L_1$ and $L_2$ for the sake of easy computation.

Let $i$, $j$, and $k$ be the three reference nodes, whose coordinate are $(x_i, y_i)$, $(x_j, y_j)$ and $(x_k, y_k)$, respectively. Let $p_i^m$, $p_j^n$ and $p_k^o$ be the least power of the beacon frames received from RNs $i$, $j$, $k$, respectively. We draw three circles whose centers are $i$, $j$, and $k$ and whose radii are $p_i^m$, $p_j^n$ and $p_k^o$, respectively. Let $I_1$ and $I_2$ be the intersection points of the circles around RNs $i$ and $j$.

Let $I_3$ and $I_4$ be the intersection points of the circles around RNs $i$ and $k$. Let $L_1$ be the line segment connecting $I_1$ and $I_2$. Let $L_2$ be the line segment connecting $I_3$ and $I_4$. The position of SN is taken to be the intersection of $L_1$ and $L_2$.

The equations of $L_1$ and $L_2$ are

$$L_1 : (2x_j - 2x_i)x + (x_i)^2 - (x_j)^2 + (2y_j - 2y_i)y + (y_i)^2 - (y_j)^2 = (p_i^m)^2 - (p_j^n)^2$$

$$L_2 : (2x_k - 2x_i)x + (x_i)^2 - (x_k)^2 + (2y_k - 2y_i)y + (y_i)^2 - (y_k)^2 = (p_i^m)^2 - (p_k^o)^2$$

The coordinate of their intersection can be obtained by solving the above two equations.
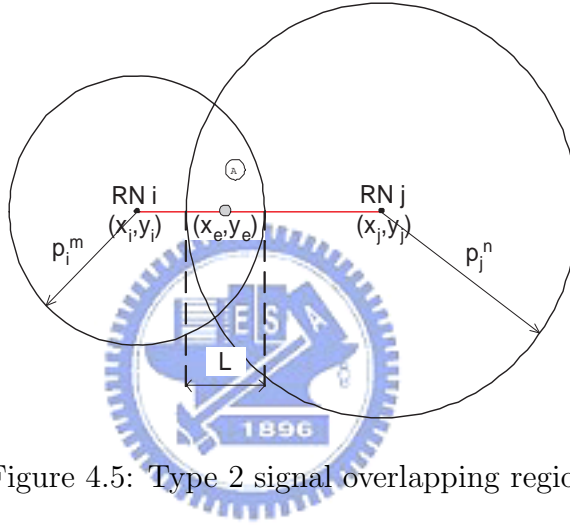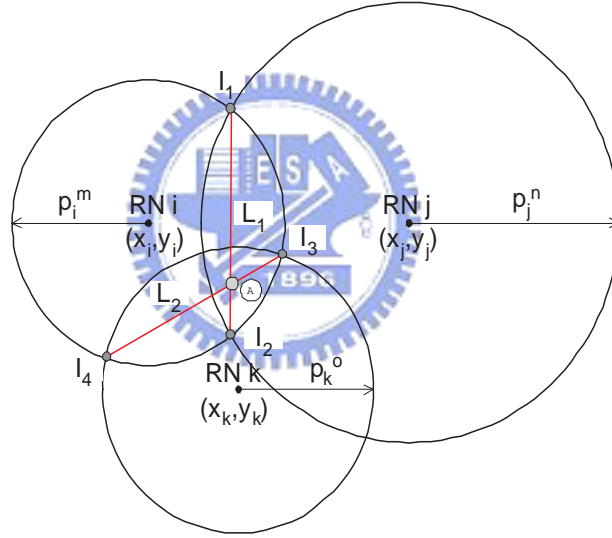


Figure 4.6: Type 3 signal overlapping region.

Type 4: The sensor nodes can receive beacon frames from $n$ reference nodes where $n \geq 4$. It is obviously that as the number of RNs increases, the computational complexity for positioning estimation also increases. Therefore, we reduce the number of heard RNs from $n$ to 4 for simply and generalization (i.e.

selecting four most "appropriate" RNs). The algorithm for selecting four appropriate RNs will be presented in later.

As shown in Figure 4.7, the position of SN is taken to be the intersection of $L_1$ and $L_2$. Let $i$, $j$, $k$, and $l$ be the four reference nodes, whose coordinate are $(x_i, y_i)$, $(x_j, y_j)$, $(x_k, y_k)$, and $(x_l, y_l)$, respectively. Let $p_i^m$, $p_j^n$, $p_k^o$, and $p_l^s$ be the least power of the beacon frames received from RNs $i$, $j$, $k$, $l$, respectively. We draw four circles whose centers are $i$, $j$, $k$, and $l$ and whose radii are $p_i^m$, $p_j^n$, $p_k^o$ and $p_l^s$, respectively. Let $I_1$ and $I_2$ be the intersection points of the circles around RNs $i$ and $k$. Let $I_3$ and $I_4$ be the intersection points of the circles around RNs $j$ and $l$. Let $L_1$ be the line segment connecting $I_1$ and $I_2$. Let $L_2$ be the line segment connecting $I_3$ and $I_4$. The position of SN is taken to be the intersection of $L_1$ and $L_2$.

The equations of $L_1$ and $L_2$ are

$$L_1 : (2x_l - 2x_j)x + (x_j)^2 - (x_l)^2 + (2y_l - 2y_j)y + (y_j)^2 - (y_l)^2 = (p_j^n)^2 - (p_l^s)^2$$

$$L_2 : (2x_k - 2x_i)x + (x_i)^2 - (x_k)^2 + (2y_k - 2y_i)y + (y_i)^2 - (y_k)^2 = (p_i^m)^2 - (p_k^o)^2$$

The coordinate of their intersection can be obtained by solving the above two equations.

Selecting the four most "appropriate" RNs is critical to the precision of estimation. There are two factors that should be considered.

First, notice that a smaller overlapped region of the circles around two RNs will result in more precise estimation. Take Figure 4.8 for example. There are three overlapped regions that are formed by circles around RN $i$ and its three neighbors ($j$, $k$, and $l$). As the overlapped region becomes smaller,
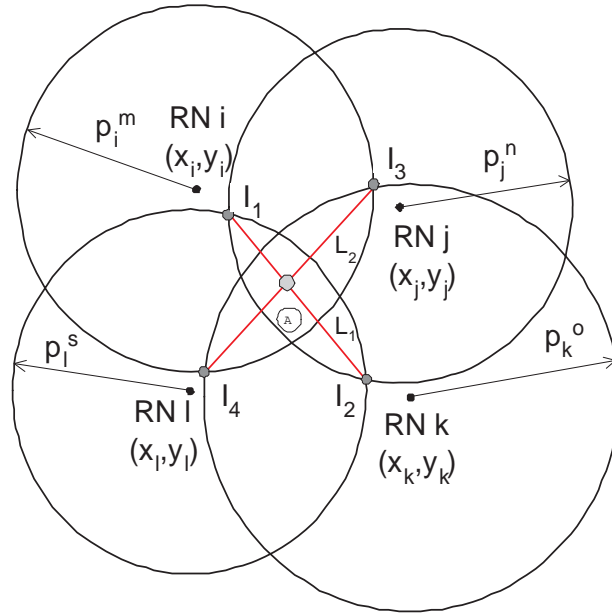
Figure 4.7: Type 4 signal overlapping region.

the average accuracy tends to decrease. So selecting the pair $(i, l)$ is more plausible than selecting either the pair $(i, j)$ or the pair $(i, k)$.

Second, the intersection of the two lines $L_1$ and $L_2$ might fall out of the overlapped region. We should be careful this situation will not occur. On the other hand, if the intersection of every pair of lines fall out of the overlapped region, we will instead choose only a line and consider this as a type-2 case. The algorithm of selecting four appropriate RNs is described in the follows.

Step 1: Compute $d_{ij} = \sqrt{(x_i - x_j)^2 + (y_i - y_j)^2}$, for all $i, j = 1, 2, \ldots, n$.

Step 2: Compute $d_{L_{ij}} = r_i + r_j - d_{ij}$, for all $i, j = 1, 2, \ldots, n$.

Step 3: Find $d_{L_{ab}} = min\{d_{L_{ij}}\}$.

Step 4: Compute $m_{ab} = (y_a - y_b)/(x_a - x_b)$.

Step 5: Compute $m_{ij} = (y_i - y_j)/(x_i - x_j)$, for all $i = 1, \ldots, n, j = i + 1, \ldots, n,$

$i \neq a$, and $j \neq b$.

Step 6: Compute

$$\theta_{ij} = cos^{-1}\left(\frac{1 + m_{ab}m_{ij}}{\sqrt{1 + (m_{ab})^2}\sqrt{1 + (m_{ij})^2}}\right),$$

for all $i = 1, \ldots, n, j = i + 1, \ldots, n, i \neq a$, and $j \neq b$.

Step 7: Choose $c$ and $d$ such that $d_{L_{cd}} = min\{d_{L_{ij}} \mid \pi/3 < \theta_{ij} < 2\pi/3 L_{ij} \neq L_{ab}\}$.
The intersection of $L_{ab}$ and $L_{cd}$ is taken as the estimated location of the SN.

Step 8: If no $L_{cd}$ satisfying the condition in (Step 7) above, estimate the SN's location with RNs $a$ and $b$ as is done in the above type-2 case.
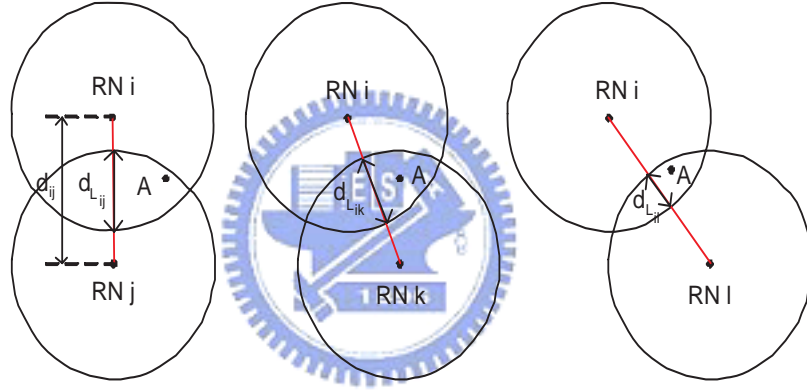


Figure 4.8: The effect of average accuracy for different overlapping regions.

## 4.3 Positioning accuracy for multiple power-levels of RNs

In order to evaluate the proposed localization mechanism, we present several experiments for four situations: failure of RNs, loss of beacon frame, unstable radio propagation model, and random placement of RNs in chapter 4.3.1 to chapter 4.3.4, respectively. The parameters for the experiments are listed in Table 4.4.
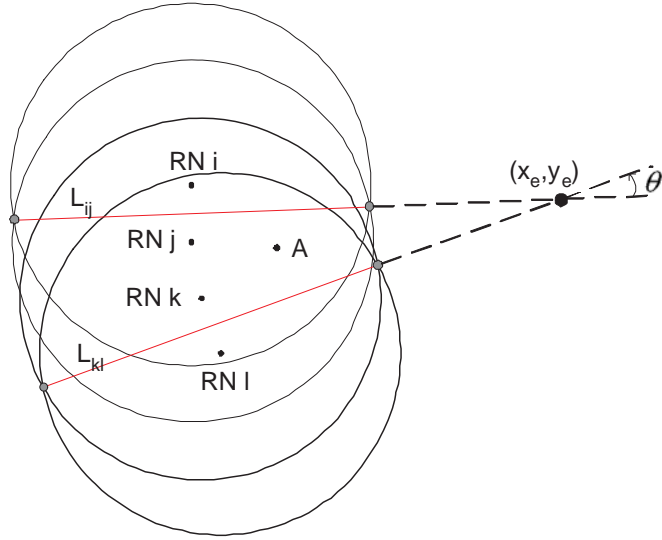
Figure 4.9: The estimated location is out of overlapping region.

Finally, we compared the positioning accuracy of proposed method with other methods [16, 17, 20] in chapter 4.3.5.

## 4.3.1   Reference nodes failure

Reference nodes broadcast beacon frames periodically to provide location information for SNs. In this experiment, we consider RN failures in a mesh structure. 100 RNs are placed in a mesh structure (that is, the vertical and horizontal distance between a pair of adjacent RNs are 100) in the $1000 \times 1000$ working area. Additionally, 10,000 SNs are also placed in a similar mesh structure in the working area. Should RNs fail, the estimation error of the locations of nearby SNs could become worse. Certain SNs cannot even be located at all because all nearby RNs have failed. Increasing the number of RNs could reduce the number of SNs that cannot be located. The number of SNs that cannot be located and the average accuracy for various RN failure rates are shown in Table 4.5.

When the RN failure rate is 10%, the number of SNs that cannot be located

59

Table 4.4: Simulation parameters.

| | RN failure | Beacon frame loss | Unstable radio propagation | Random placement of RNs |
|---|---|---|---|---|
| Power levels | (47, 69, 85, 99) | (47, 69, 85, 99) | (47, 69, 85, 99) | (47, 69, 85, 99) |
| Number of RNs | 100 | 4 (at corner) | 4 (at corner) | (100,200,300, 400,500) |
| Sensor nodes | 10,000 | 10,000 | 10,000 | 10,000 |
| Working area | 1000×1000 | 100×100 | 100×100 | 1000×1000 |
| Failure rate | (0%, 1%, 5%, 10%, 20%) | 0% | 0% | 0% |
| Loss rate | 0% | (0%, 1%, 5%, 10%, 20%) | 0% | 0% |
| Propagation model | Ideal | Ideal | Unstable | Ideal |
| Network structure | Mesh | Mesh | Mesh | Random |

is 280 and the average accuracy is 0.1204. The average accuracy for various RNs failure rates is shown in Figure 4.10.

Table 4.5: The average accuracy for RNs failure.

| RNs Failure(%) | Un-locate SNs | Avg. error | Avg. accuracy |
|---|---|---|---|
| 0% | 0 | 5.8686 | 0.0593 |
| 1% | 2 | 6.425 | 0.0649 |
| 5% | 66 | 8.7686 | 0.0886 |
| 10% | 280 | 11.917 | 0.1204 |
| 20% | 1310 | 18.4823 | 0.1867 |

## 4.3.2 Beacon frame loss

In a wireless network, a channel can only be used for a single pair of SNs at any time. Given the limited number of channels, beacon signals are frequently lost due to signal collisions. In this experiment, we study the effect of beacon frame
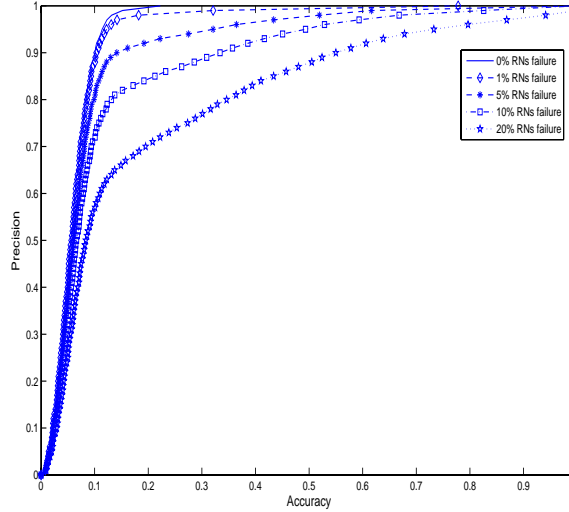
Figure 4.10: The average accuracy for various RNs failure rates.

loss. We tested four beacon frame loss rate: 1%, 5%, 10% and 20%. There are four RNs, which are deployed in the four corners of the $100 \times 100$ mesh area. Table 4.6 shows the average accuracy under various beacon frame loss rates. When the beacon frame loss rate is no more than 5%, the average accuracy increases slightly. When the rate exceeds 5%, the average accuracy becomes intolerable.

There are two approaches to reduce the beacon frame loss. One utilizes random backoff or the frequency-division mechanism to reduce beacon collision. The other is for the sensor node to listen for a period of time to collect enough beacon frames. Figure 4.11 is the average accuracy relative to the beacon frame loss rate. When the rate is 10%, our method gives 80% (90%) average accuracy to within 0.16 (0.21). Even when the rate is 20%, our method gives almost 100% accuracy to within 0.41.

Table 4.6: The average accuracy for beacon loss.

| Beacon frame loss rate | Avg. error | Avg. accuracy |
| --- | --- | --- |
| 0% | 5.8686 | 0.0593 |
| 1% | 6.0916 | 0.0615 |
| 5% | 6.9899 | 0.0706 |
| 10% | 8.161 | 0.0824 |
| 20% | 10.6502 | 0.1076 |

### 4.3.3 Unstable radio propagation model

In reality, the coverage of RNs is irregular due to the multipath propagation effect. In order to evaluate the performance of our method under unstable radio propagation, the shadowing model [25] is considered. The shadowing model can be represented by

$$[\frac{P_r(d)}{P_r(d_0)}]_{dB} = -10\beta \log(\frac{d}{d_0}) + X_{dB}$$

where $P_r(d)$ is the power of the received signal at distance $d$, $\beta$ is the path loss exponent, and $X_{dB}$ is a Gaussian random variable (with $\mu = 0$ and standard deviation $\sigma_{dB}$). $X_{dB}$ accounts for the random effect on radio propagation caused by the environment. Note that the shadowing model extends the ideal circle model to a statistic model.

In this experiment, there are four RNs deployed at the four corners of the $100 \times 100$ working area. 10,000 SNs are organized into a mesh, similar to the first experiment. Table 4.7 shows the average accuracy relative to $\sigma_{dB}$. When $\sigma_{dB}$ is less than 3, the average accuracy is less than 0.17. This means that our method is applicable in modestly unstable radio-propagation environments.

The unstability in radio propagation causes more serious effect in our localiza-
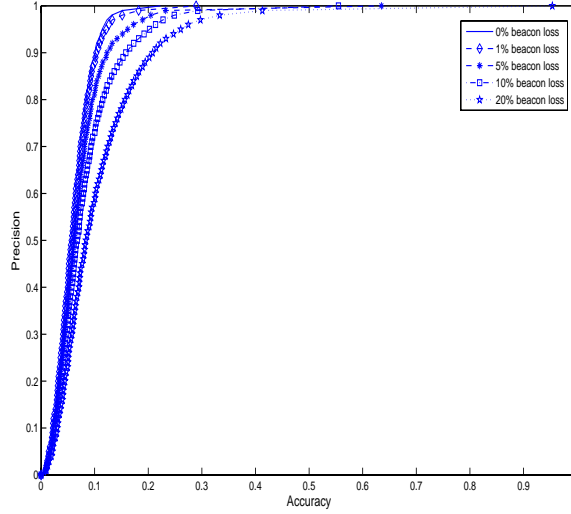
Figure 4.11: The average accuracy for various beacon frame loss rates.

tion algorithm than RN failures and beacon frame losses. Figure 4.12 shows the average accuracy in the shadowing model. When $\sigma_{dB}$ is 3, our method gives 90% accuracy to within 0.3 units distance.

Table 4.7: The average accuracy for various $\sigma_{dB}$ with $\beta = 2$ in shadowing model.

| $\sigma_{dB}$ | Avg. error | Avg. accuracy |
|---|---|---|
| 1 | 6.397 | 0.0646 |
| 2 | 10.058 | 0.1056 |
| 3 | 16.7451 | 0.1691 |
| 4 | 24.0704 | 0.2431 |
| 5 | 29.9701 | 0.3027 |

63

Figure 4.12: The average accuracy for various standard deviation with $\beta = 2$ in shadowing model.

## 4.3.4 Random placement of reference nodes

In the above three simulations, we consider only the mesh deployment of RNs and SNs. In this simulation, RNs are randomly deploy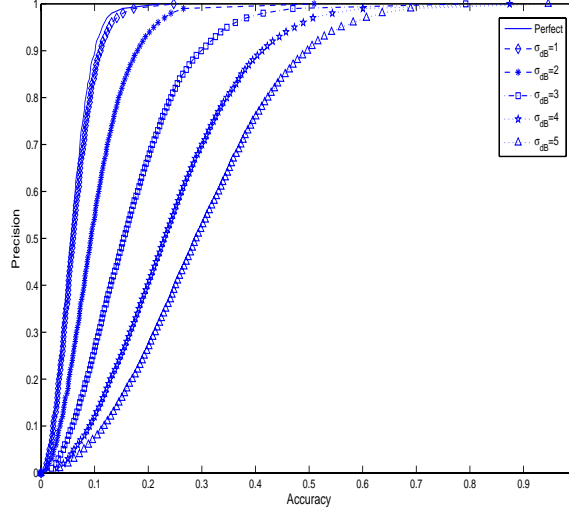ed in a $1000 \times 1000$ square area. Table 4.8 shows the average accuracy relative to the number of deployed RNs. The average accuracy is roughly in inverse proportion to the number of RNs. When the number of RNs is too few, say 100, a significant part of the sensing are is not covered by any RN. Hence, many SNs cannot be located. When the number of RNs (say 500) is enough to cover the whole sensing area, all nodes can be located and the average accuracy is only 0.0703. We can use a density control algorithm to evenly distribute RNs so that the average accuracy can be reduced. Figure 4.13 shows the average accuracy for various numbers of RNs. When the number of RNs is 300, our method gives 90% accuracy to within 0.23 unit distance. The reduction in the average accuracy (by increasing RNs) becomes less obvious when

the number of RNs exceeds 300.

Table 4.8: The average accuracy with random placement of RNs.

| Number of RNs | Un-located SNs | Avg. error | Avg. accuracy |
|---|---|---|---|
| 100 | 722 | 30.9267 | 0.3124 |
| 200 | 80 | 15.5353 | 0.1569 |
| 300 | 11 | 10.0668 | 0.1017 |
| 400 | 2 | 8.2485 | 0.0833 |
| 500 | 0 | 6.957 | 0.0703 |

### 4.3.5  Comparison with other positioning methods

We consider the simulation environment that RNs are randomly deployed in a 1000*1000 working area for variety of number of RNs. For the same simulation environment, the average accuracy of centroid method [16], range-free method [17], and our method are shown in Figure 4.14. These methods are range-free positioning methods that utilize the beacon signal to estimate node's position without ranging technologies. For 100 RNs, the average accuracy of these positioning methods is larger than 0.3. As the number of RNs increase, the average accuracy of them can be improved.

The average accuracy of proposed method is slightly better than others besides the simulation environment of 200 RNs. In low density of RNs (i.e. number of RNs < 300), the entire working area cannot be covered by all RNs that was deployed randomly. Because the uncovered area cause the area-based positioning method failed to work, the improvement of average accuracy is limited. In high density of
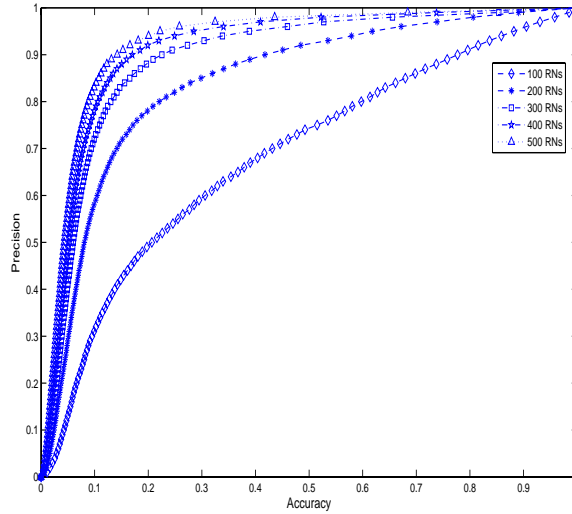
65

Figure 4.13: The average accuracy for various numbers of RNs with random deployment strategy.

RNs, range-free and cell-based methods are almost the same.

However, the range-free positioning method uses the approximate point-in-triangulation test (APIT) algorithm to estimate node's location. This algorithm calculates the center of gravity of the intersection of all of the triangles to determine its estimated position. Note that the triangle is formed by selecting heard RNs in which a SN resides. For high density of RNs, the computation cost of APIT is higher than our method. Therefore, considering the computation power, complexity of positioning algorithm, and positioning accuracy, our method is better than others.
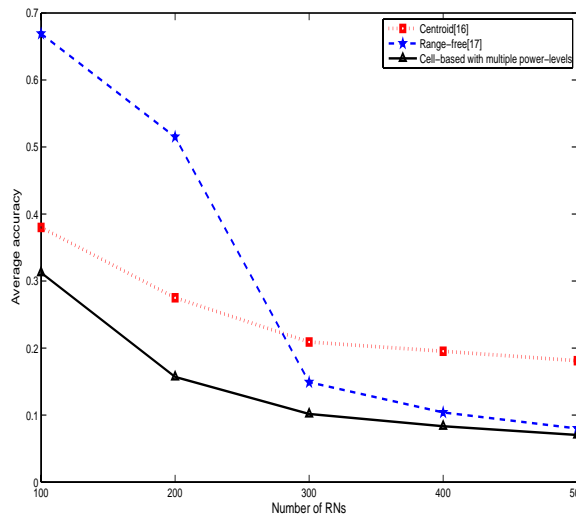
66

Figure 4.14: The average accuracy of centroid[16], range-free[17] and proposed positioning methods for various numbers of RNs.

# Chapter 5

# Conclusion

We proposed a cell-based positioning method with single power level for wireless networks. In our method, a set of RNs with overlapping regions of coverage are arranged in a regular (hexagonal) structure [14] and irregular (random) structure [29] and broadcast the beacon frames. Sensor nodes only collect the beacon frames from RNs and use the localization data in the beacon frame to calculate their locations. The worst-case and average-case accuracy are analyzed with perfect RNs and ideal radio model. For reality, unstable radio model and imperfect RNs are considered. The simulation results show that the proposed method worked well in the outdoor, shadowed urban area. Cell-based positioning method with backup RNs is also presented to reduce the number of un-located SNs when one or more RNs are failed. We have implemented our positioning method on a sensor network test bed to verify its feasibility [24].

In order to improve the positioning accuracy, an extension of cell-based positioning method, multiple power-levels approach for wireless network positioning, is proposed. It uses simple algorithm without additional device to locate sensor nodes. In addition, we proposed an equal-area ring strategy setting up the power-level set to provide the higher average accuracy. The average accuracy using this

strategy is similar to the one using optimal power-level set that is obtained by brute-force approach. By simulation, using four power-levels in ideal propagation model, the average accuracy is less than 0.07 unit distance. The robustness of proposed algorithm is shown by simulation that contains the factor of reference node failure, beacon frame loss, and unstable radio environment.

The main advantages of the proposed method are that (1) the proposed method is a distributed positioning method; (2) sensor node requires little computation to localize by itself; (3) it is suitable for wireless networks, especially for wireless sensor networks, for low cost and easy computation; (4) it has high average accuracy; and (5) it is suitable for real world applications.

The following directions might be interesting for possible future work:

- Find an optimal layout for irregular network structure by tuning RNs' transmitting power.

- Find a power-saving mechanism to prolong lifetime of RNs.

- Find a secure message communication and positioning estimation algorithm for untruthful environment.

# Bibliography

[1] N. Davies, K. Cheverst, K. Mitchell, and A. Efrat, "Using and determining location in a context-sensitive tour guide," *IEEE Computer Magazine*, vol. 34, Aug. 2001 pp. 35-41.

[2] D. Cotroneo, S. Russo, F. Cornevilli, M. Ficco, and V. Vecchio, "Implementing positioning services over an ubiquitous infrastructure," *Proceedings of the Second IEEE Workshop on Software Technologies for Future Embedded and Ubiquitous Systems*, May 2004, pp. 14-18.

[3] I. F. Akyildiz, W. Su, Y. Sankarasubramaniam, and E. Cayirci, "Wireless sensor networks: A survey," *Computer Network*, vol. 38, pp. 393-422, 2002.

[4] M.Voddiek, L. Wiebking, P. Gulden, J. Wieghardt, C. Hoffmann, and P. Heide, "Wireless local positioning," *IEEE Microwave Magazine*, vol. 4, pp. 77-86, Dec. 2004.

[5] J. Hightower and G. Borriello, "Location Systems for Ubiquitous Computing," *IEEE Computer*, vol. 34, no. 8, pp. 57-66, Aug. 2001.

[6] B. Hofmann-Wellenhof, H. Lichtenegger, and J. Collins, "Global Positioning System: Theory and Practice", fifth edition , Springer Verlag, 2001.

[7] R. Want, A. Hopper, V. Falcao and J. Gibbons, "The Active Badge Location System," *ACM Trans. on Information Systems*, Jan. 1992, pp. 91-102.

[8] A. Harter, A. Hopper, P. Steggles, A. Ward, P. Webster, "The Anatomy of a Context-Aware Application," Proc. 5th Ann. Intl Conf. Mobile Computing and Networking (Mobicom 99), ACM Press, New York, 1999, pp. 59-68.

[9] N.B. Priyantha, A. Chakraborty, and H. Balakrishnan, "The Cricket Location-Support System," Proc. 6th Ann. Intl Conf. Mobile Computing and Networking (Mobicom 00), ACM Press, New York, 2000, pp. 32-43.

[10] P. Bahl and V. N. Padmanabhan, "RADAR: An in-building RF-based user location and tracking system," *in Proc. IEEE Annu. Joint Conf. IEEE Computer and Communications Societies (INFOCOM'00)*, 2000, pp. 775-784.

[11] J. Hightower, R. Want, and G. Borriello, SpotON: An Indoor 3d Location Sensing Technology Based on RF Signal Strength, UW CSE 2000-02-02, Univ. Washington, Seattle, Feb. 2000.

[12] G. M. Djuknic, and R. E. Richton, "Geolocation and assisted GPS," *IEEE Computer Magazine*, vol. 34, pp. 123-125, Feb. 2001.

[13] L. Doherty, K. S. J. Pister, and L. E. Ghaoui, "Convex position estimation in wireless sensor networks," *In Proc. of INFOCOM*, vol. 3, pp. 1655-1663, 2001.

[14] H.-C. Chu and R.-H. Jan, "A Cell-Based location-sensing method for wireless networks", *Wireless Communication and Mobile Computing*, vol. 3, pp. 455-463, 2003.

71

[15] S. Capkun, M. Hamdi, and J. P. Hubaux, "GPS-free positioning in mobile ad hoc networks," in Proc. 34th Annu. Hawaii Int. Conf. System Sciences, 2001, pp. 3481-3490.

[16] N. Bulusu, J. Heidemann and D. Estrin. "GPS-less low cost outdoor localization for very small devices." *IEEE Personal Communications Magazine*, vol. 7, no. 5, pp. 28-34. Oct., 2000.

[17] T. He, C. Huang, B. Blum, J. Stankovic, and T. Abdelzaher, "Range-free localization schemes in large scale sensor networks," in Proc ACM/IEEE 9th Annu. Int. Conf. Mobile Computing and Networking (MobiCom'03), 2003, pp. 81-95.

[18] F. Mondinelli and Z.M. Kovacs-Vajna, "Self localizing sensor network architectures," *PIEEE Transactions on Instrumentation and Measurement*, vol. 53, Apr. 2004, pp.277-283.

[19] Chong Liu, Kui Wu, and Tian He, "Sensor localization with Ring Overlapping based on Comparison of Received Signal Strength Indicator," *IEEE International Conference on Mobile Ad-hoc and Sensor Systems (MASS)*, Oct. 2004, pp. 516-518.

[20] D. Niculescu and B. Nath, "Localized positioning in ad hoc networks," *Ad hoc Networks*, vol. 1, Sep. 2003, pp. 2476-259.

[21] D. Niculescu and B. Nath, "Ad hoc positioning system (APS) using AoA," in Proc. IEEE Joint Conf. IEEE Computer Communications Societies (INFOCOM), Mar. 2003, pp. 1734-1743.

[22] W. Ruml, Y. Shang, and Y. Zhang, "Location from mere connectivity," in Proc. 4th ACMInt. Symp. Mobile Ad Hoc Networking and Computing (MobiHOC'03), 2003, pp. 201-212.

[23] K.-F. Ssu, C.-H. Ou, and H. C. Jiau, "Localization with mobile anchor points in wireless sensor networks," IEEE transactions on Vehicular Technology, vol. 54, no. 3, pp. 1187-1197, May 2005.

[24] H.-C. Chu and R.-H. Jan, "A GPS-less, outdoor, self-positioning method for wireless sensor networks", accepted and to appear in Journal of Ad Hoc Networks, 2006.

[25] T. S. Rappaport, "Wireless communications, principles and practice," 2nd edition, Prentice Hall, 2002.

[26] Network Simulator ns-2: Documentation, Chapter 18 Radio propagation models, http://www.isi.edu/nsnam/ns/ns-documentation.html, Nov. 2005.

[27] P. J. M. van Laarhoven and E. H. L. Aarts, "Simulated annealing: theory and applications", Dordrecht, D. Reidel, 1987.

[28] T.M. Mote, http://www.xbow.com/Products/productsdetails.aspx?sid=72.

[29] R.-H. Jan, H.-C. Chu, and Y.-F. Lee, "Improving the accuracy of cell-based positioning for wireless networks", *Computer network*, vol. 46, pp. 817-827, Dec. 20, 2004.

# Vita

**Hung-Chi Chu** received the B.S. and M.S. degrees in Computer Science and Engineering from Tatung University, Taiwan, in 1995, and 1997, respectively. From 1999 to 2001, he was a research assistant in the Department of Computer Center at Tatung University developing Campus Administration System. Currently, he is finishing his Ph.D. program in the Department of Computer Science at National Chiao Tung University. His research interests include wireless networks, wireless sensor networks, and artificial intelligence.

# Publication List

## Journal Papers

[1] **Hung-Chi Chu,** and Rong-Hong Jan, "A cell-based location-sensing method for wireless networks," *Wireless Communications and Mobile Computing*, vol. 3, no. 4, pp. 455-463, 2003. (SCI)

[2] Rong-Hong Jan, **Hung-Chi Chu**, and Yi-Fang Lee, "Improving the accuracy of cell-based positioning for wireless networks", *Computer networks*, vol. 46, pp. 817-827, Dec. 20, 2004. (SCI, EI)

[3] Yu-He Gau, **Hung-Chi Chu**, and Rong-Hong Jan, "A Weighted Multilateration Positioning Method for Wireless Sensor Networks" accepted and to appear in International Journal of Pervasive Computing and Communications, 2006.

[4] **Hung-Chi Chu** and Rong-Hong Jan, "A GPS-less, outdoor, self-positioning method for wireless sensor networks," accepted and to appear in Ad Hoc Networks, 2006. (EI)

[5] Jen-Yu Fang, **Hung-Chi Chu**, Rong-Hong Jan, "A multiple power-level approach for wireless sensor-network positioning," submitted to IEEE Transactions on Vehicular Technology.

## Conference Papers

[1] **Hung-Chi Chu** and Rong-Hong Jan, "Cell-Based positioning method for wireless networks," Proceeding of the International Conference on Parallel and Distributed Systems(ICPDS), pp. 232-237, National Central University, Taiwan, Dec. 17-20, 2002.

[2] Rong-Hong Jan, **Hung-Chi Chu** and Yi-Fang Lee, " Improving the accuracy of Cell-Based positioning for Wireless Networks," Proceeding of the International Conference on Parallel and Distributed Computing and Systems(ICPDCS), pp. 375-380, CA, USA, Nov. 3-5, 2003. (EI)

[3] **Hung-Chi Chu** and Rong-Hong Jan, "A GPS-less positioning method for sensor networks," The 1st International Workshop on Distributed, Parallel and Network Applications(DPNA), vol. 2, pp. 629-633, Fukuoka, Japan, Jul. 20-22, 2005. (EI)

[4] Yu-He Gau, **Hung-Chi Chu**, and Rong-Hong Jan, "A Weighted Multilateration Positioning Method for Wireless Sensor Networks," Workshop on Wireless, Ad Hoc, and Sensor Networks(WASN), National Central University, Session A1, pp.3-8, Taiwan, Aug. 1-2, 2005.